UNIVERSITY OF THESSALY
SCHOOL OF ENGINEERING
DEPARTMENT OF MECHANICAL ENGINEERING

EFFECT OF PERMEABILITY IN PRESSURE PROFILE OF THREE POROUS ZONES OF ARTICULAR CARTILAGE

by

IOANNA DELEMISSI

Submitted in partial fulfillment of the requirements for the degree of Diploma in Mechanical Engineering at the University of Thessaly

Volos, 2022

UNIVERSITY OF THESSALY
SCHOOL OF ENGINEERING
DEPARTMENT OF MECHANICAL ENGINEERING

EFFECT OF PERMEABILITY IN PRESSURE PROFILE OF THREE POROUS ZONES OF ARTICULAR CARTILAGE

by
IOANNA DELEMISSI

Submitted in partial fulfillment of the requirements for the degree of Diploma in Mechanical Engineering at the University of Thessaly

Volos, 2022

Approved by the Committee on Final Examination:

Advisor	Dr. Athanasios Papathanasiou, Professor, Department of Mechanical Engineering, University of Thessaly
Member	Dr. Andreas Tsiantis, Department of Mechanical Engineering, University of Thessaly
Member	Dr. Alexis Kermanidis, Associate Professor, Department of Mechanical Engineering, University of Thessaly

Date Approved: [Month dd, yyyy]

Acknowledgements

I would like to start by expressing my gratitude to some of the people I met, collaborated with and who played a significant role in the elaboration of my Diploma Thesis. First of all, I would like to thank the Supervisor of my Thesis, Professor Dr. Athanasios Papathanasiou for his great support, invaluable help and guidance during my work. I'm also grateful to the other members of my dissertation's examination committee, Professors Dr. Andreas Tsiantis and Dr. Alexis Kermanidis, for their invaluable support and careful review of my work.

I would also like to express my gratitude to Mr. Lefteris Benos who inspired me for the topic of my Diploma Thesis and helped me greatly with his knowledge in the bioengineering field.

Finally, I would like to express my heartfelt thanks to my best friends, Katerina and Christina who were something more than my second family all these years, to Filia and to all the people who contributed to the beautiful moments and unique experiences we shared throughout our student years. I would like to dedicate my Thesis to my family for their everlasting love and support throughout the years.

EFFECT OF PERMEABILITY IN PRESSURE PROFILE OF THREE POROUS ZONES OF ARTICULAR CARTILAGE

IOANNA DELEMISSI
Department of Mechanical Engineering, University of Thessaly

Supervisor: Dr Athanasios Papathanasiou
Professor of Operational Research in area of Energy, Industrial Processes & Pollution Abatement Technology

Abstract

In this Diploma Thesis, the flow through a fibrous porous medium, which is used as a model to represent the Articular Cartilage (AC) of the knee joint, is simulated using the open-source OpenFOAM computing environment. Our objective is to investigate the effect of the AC microstructure, represented by spatially variable permeability fields, on fluid transfer and pressure development within the three porous zones comprising a typical Articular Cartilage. An analytical solution is developed for the case of an isotropic medium and was used as a benchmark against the numerical results from the simulations of the three anisotropic porous zones of AC; we found a consistently good agreement between numerical and analytical solutions. The permeability models that have been used in the simulations are represented and explained in detail. Finally, simulations were carried out which elucidated the effect of the thickness of each zone of AC in the force distribution in the top surface of AC.

Contents

LIST OF TABLES

LIST OF FIGURES

CHAPTER 1. INTRODUCTION

1.1 Knee Joint

The knee is a complicated and vulnerable structure and one of the largest hinge joints in the human body. It is the most affected joint by osteoarthritis. Every day knee is subjected to significant biomechanical stresses as lifting and kneeling and from other activities, therefore it is a common site of injury. Knee permits four main movements, extension, flexion, lateral and medial rotation. It is categorized as a hinge type synovial joint that allows flexion, extension and rotation and provide complete stability and control, under a wide range of loading conditions. The knee consists of 2 joints (articulations), a tibiofemoral where the tibia meets the femur and a patellofemoral where the patella meets the femur. It is comprised of by 4 bones, cartilage and a large system of ligaments, tendons and other tissues. The bone architecture of the femur, tibia, and patella and fibula provide stability of the knee joint, together with static and dynamic restraints of the ligaments, capsule, and musculature crossing the joint.

The tibiofemoral joint is the largest joint in the body, and is an articulation between the lateral and medial condyles of the distal end of the femur and the tibial plateaus, both of which are protected by a thick film of hyaline cartilage. The patellofemoral joint is a saddle joint shaped by the articulation of the patellar surface of femur and the posterior surface of patella. This joint is important to knee stability essential through its function in the extensor mechanism. Both joint surfaces are covered with a hyaline cartilage (articular cartilage) for which we will emphasize later.

Ligaments are attached to bones and provide stability, strength and restrict the forward and backward movement of the tibia. Ligaments are made of collagen, connective tissue and elastic fibers that are slightly stretchy. In knee joint there are two main types of ligaments, collateral and cruciate. Collateral ligaments consist of medial collateral ligament

(MCL) which is on the inside side of the knee and attaches the thigh bone (femur) to the shin bone (tibia) and of lateral collateral (LCL) which is on the outside and connects the femur to calf bone. Furthermore, cruciate ligaments control the front and back motion of the knee and consist of the anterior ligament (ACL) and the posterior ligament (PCL). There are two main muscle groups that surround the knee – hamstrings and quadriceps. Quadriceps are located on the front of the thighs and the hamstring on the back of the thighs. Muscles help the motion of the knee, and they provide stability and well alignment in coordination with ligaments. The elastic tissue that helps the connection between the muscles and the bones of the knee are called tendons and they are made up of collagen. Menisci are fibrocartilage structures that are flattened at the center of the knee joint and cover each bone. They deepen the articular surface into which the femur attaches with them, and they also act as shock absorbers and may be cracked when the knee is powerfully bend or rotated.

In Figure 1 we can see how the anatomy of knee joint structure is.

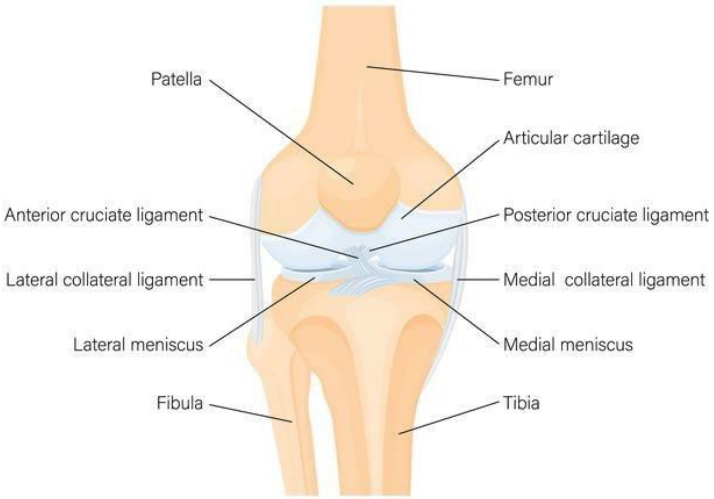

Figure 1. *Knee joint structure,* [1].

1.2 Articular Cartilage

While there are many important components of the knee joint as we mention above, articular cartilage is the primary focus of this Thesis. The knee is a crucial load-bearing joint, which differs from the other major load-bearing joints in those soft tissues, rather than articular shape, are the important stabilizing factors, [2]. Articular cartilage (AC) is a popular objective for researchers due to its importantly poor self-renewal ability.

AC is a flexible and avascular loadbearing tissue that covers the interacting bone surfaces in diarthrodial joints. The thickness of AC it's about 2–4 mm, [3]. It is composed of an extracellular matrix (ECM) which is composed of collagen, water, proteoglycans and in a lesser number of proteins and glycoproteins, with a sparse distribution of highly specialized cells called chondrocytes. These components are organized and arranged in a way that is maximally adapted for biomechanical properties and the mechanical and biological functions vary zonally, [4]. From a mechanical standpoint, AC can be seen of as a composite material that provides a variety of critical biomechanical properties for knee joint motion. It allows for easy articulation, increased weight distribution, and shock absorption while it distributes joint loads over a large area, reducing the stresses sustained by the contacting joint surfaces. When articulation is smooth, less stress is applied on the cartilage surface and the tissue does not wear out easily. Thanks to elastic form of cartilage tissue, it gives rise to deformations, but always comes back to its initiate shape. Due to the complex composition and structure of the cartilage, the properties of AC are depth-dependent and strain-dependent ([5], [6]).

1.3 Composition of Articular Cartilage

AC is composed of highly specialized cells called chondrocytes and of a dense extracellular matrix (ECM). The ECM is primarily composed of matrix water, proteoglycans, collagen fibers, and some mineral materials. Table 1 shows an overview of the general composition of the articular cartilage in more detail, [7].

Table 1. *Composition of Knee Articular Cartilage in human body,* ***[7]*** *.*

Chondrocytes	1-10%
Water	70-80%
Collagen	12-14%
- Type II	10-12%
- Type IX	~ 1%
- Type XI	~ 1%
Proteoglycans	7-9%
- Hyaluronic acid—proteoglycan—aggregates	6-8%
- Other proteoglycans	~ 1%
Mineralic materials	<4%
Matrix proteins	<1%

Chondrocytes are highly specialized and metabolically active cells and the only cell type in AC. Chondrocytes set up the collagen, proteoglycans, and non-collagenous proteins within a highly specialized tissue, suitable for carrying out important functions. They receive nutrients through diffusion from the synovial fluid, which is rich in proteins derived from the blood plasma, and from the joint tissues (hyaluronic acid, PRG4), [3]. Chondrocytes depending on the zonal regions, vary in shape, size, and number.

Collagen is the most abundant structural macromolecule in ECM, and it makes up about 60% of the dry weight of cartilage. Collagen content remains fairly constant with depth, but fiber orientation varies from parallel to the surface in the superficial zone, to perpendicular in the deep zone, [8]. The elasticity of the collagen network depends on the intramolecular and intermolecular connections among the fibrils. The most significant characteristic of collagen fibers is their tensile strength, while they will deform when they will be compressed and their capability to contain the swelling pressure of the proteoglycans. Furthermore, collagen is responsible for the outer shape of the cartilage and its form. Type II collagen represents 90% to 95% of the collagen in ECM and forms fibrils and fibers intertwined with proteoglycan aggregates and supplies a tensile strength to the cartilage. Collagen types I, IV, V, VI, IX, and XI are also present but contribute only a minor proportion, [7]. The structure of the fibers is thought to strongly linked to their function in the tissue,

and it has been thought that they constitute the major source of anisotropy in the elastic properties (Farquhar et al. [9], Soulhat et al. [10], Ogden [11], Federico et al., [12]).

Below, in Table 2 we can see the importance of the role of each type of collagen in AC from A. M. Bhosale and J. B. Richardson, [3].

Table 2. *Different types of collagen and their functions,* ***[3]****.*

Collagen type	Morphological location	Function
II	Principal component of microfibril (90-95%)	Tensile strength
VI	Pericellular matrix	Helps chondrocytes to attach to the matrix
IX	Cross-linked to surface of microfibril	Tensile properties and inter-fibrillar connections
X	Closely related to the hypertrophied cells in calcified cartilage layer	Structural support and aids in cartilage mineralization
XI	Within or on macrofibrils	Nucleates fibril formation

AC is a highly hydrated tissue since water contributes up to 80% of its wet weight. Consequently, AC must be considered as a biphasic (two phase) material. The biphasic theory of the cartilage has been described first from Mow et al., [13]. In particular, the solid phase is examined as a porous permeable fiber reinforced phase and the fluid phase as a freely flowing phase. Water flows through the porous solid matrix and the mechanical properties and permeability of the tissue depends highly on the concentration of the ECM component (Mow et al. [13], Gannon et al. [14]). Inorganic ions such as sodium, calcium, chloride, and potassium are dissolved in the tissue water. The flow of water through the cartilage and across the articular surface helps to transport and distribute nutrients to chondrocytes, in addition to providing lubrication, [15]. The flow of the fluid inside the AC has long been identified as a crucial component of articular cartilage function where we will mention and analyze later.

Synovial fluid or joint fluid is a viscous, non-Newtonian fluid located between human joints including knees, hips, shoulders, hands and feet. A normal knee joint is bathed in a thin fibrous tissue only, slippery liquid which consists of filtrate plasma and hyaluronic acid

and few cells thick that is inside the synovial membrane. A usual synovial fluid is characterized by high viscosity due to hyaluronic acid. The two main roles of synovial fluid are to lubricate the joint due to its high in water capacity and to nourish the cartilage. Joint fluid reduces the friction during the movements of the knee and nourishes the articular cartilage by letting nutrients to penetrate it and by blocking the passage of harmful substances. During the four main motions of the knee the synovial fluid that is captivated in the articular cartilage, is squeezed out to sustain a layer of fluid on the cartilage surface and provides protection and support to the joint.

Proteoglycans represent the second-largest group of macromolecules in the ECM and account for 10% to 15% of the wet weight. Proteoglycans consist of a protein core with 1 or more linear glycosaminoglycan chains covalently attached, [4]. Articular cartilage contains a variety of proteoglycans that are vital for normal function, but the vast majority are aggrecans.

1.4 Structure of Articular Cartilage

The mechanical properties, and consequently the function of cartilage, are determined by the interactions of its matrix constituents. If the organization and composition of cartilage varies with depth, its mechanical properties also vary accordingly.

AC is an anisotropic tissue divided morphologically into four named layers (zones) with different biomechanical and biochemical functions, namely the superficial or tangential zone, middle or transitional zone, deep or radial zone and the calcified zone. According to Clark [16], and Kaab et al. [17]. AC is depth-dependent: oriented to merge with the articular surface in the superficial zone (SZ), perpendicular to the boundary between bone and cartilage in the deep zone (DZ), and randomly oriented in the middle zone (MZ). Each of these zones possesses unique structural, functional and mechanical properties and chondrocytes in different zone produce specific responses to different stimuli by secreting different proteins. From the top zone (SZ) to the deep zone (DZ), the individual zones are mainly classified by chondrocyte cell density and morphology, collagen fibrils orientation and ECM composition. Below in Figure 2, we can see how AC is structured in these four zones and we describe each zone in detail, [18].

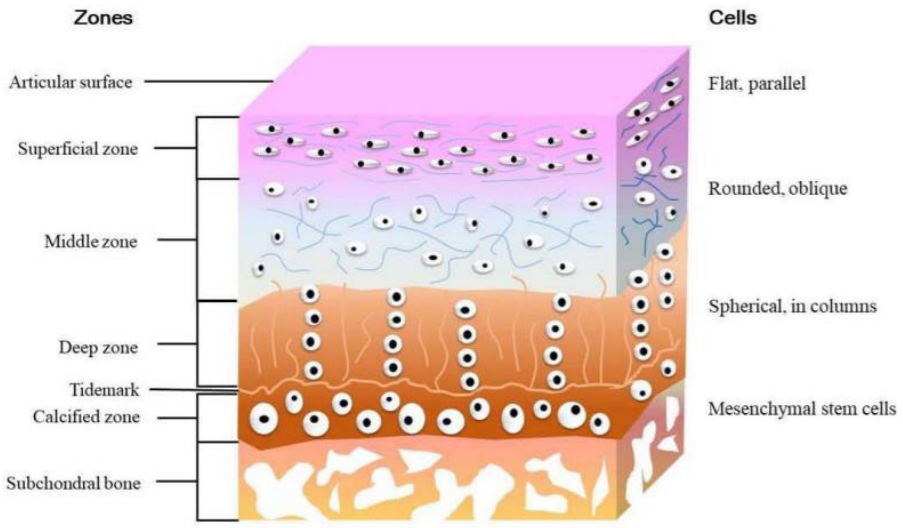

Figure 2. *Structure of articular cartilage zones,* [18].

Superficial zone

The superficial zone has various obvious structural features, playing a significant role in its unique mechanical properties and behavior. Superficial zone accounts for the 10% to 20% of total cartilage thickness. Collagen fibrils in this zone are thin and oriented parallel to the AC surface. This fibril orientation provides a greatest tensile and shear strength in this zone. Chondrocytes in the most of this zone are flattened, small and ellipsoid cells and they have a higher density in comparison with other cells in the matrix. Generally, cells in superficial layer are not very active and as a result there is a little wear out. Also, the superficial zone is the most hydrated of all zones with a low concentration of proteoglycans and acts as a barrier for the large molecules (antibodies). Its import to mention that a disorder of this zone can change the mechanical properties of the articular cartilage and consequently contributes to the progress of osteoarthritis. More specific, with a distribution of this zone the permeability of the tissue will increase, leading to greater fluid exchange of the cartilage with its surroundings and during compression, this leads to greater mechanical stress on the macromolecular network, [19].

Middle zone

Middle zone represents 40% to 60% of the total AC volume and it's the bridge between the superficial zone and the lower ones. The collagen fibrils in this layer are thicker and they are oriented randomly (obliquely) to the AC surface. The shape of the chondrocytes is spherical, and cells have a lower density in this zone. Furthermore, proteoglycan aggrecan concentration is higher in this zone, [3]. Functionally, the middle zone is the first line of resistance against compressive forces, [3], [5].

Deep zone

Deep zone accounts for about of the 30% of articular cartilage volume. In this zone collagen fibrils have the largest diameter, and they are arranged perpendicular to the surface; therefore, deep layer supplies the cartilage with a great resistance to compressive forces. The chondrocytes have a spheroidal shape, and they are typically arranged in columnar orientation, parallel to the collagen fibers and perpendicular to the joint line. Also, we have here the highest proteoglycan content, and the lowest water concentration, [4].

Calcified zone

The calcified zone plays an integral role in securing the cartilage to bone by anchoring the collagen fibrils of the deep zone to subchondral bone, [4]. It contains collagen type X and its responsible for providing important structural integrity and provide a shock absorber along with the subchondral bone. In this zone, the cell population is scarce, and chondrocytes are hypertrophic, [4]. For this reason, this zone has a low metabolic activity.

In summary, the four zones of cartilage play a significant role and differ in many aspects. Cellular density is highest at the superficial layer of the articular cartilage and progressively decreases through the intermediate and deep zones to about one-third the density of the superficial layer. Also, a greater range of fibril diameters is seen in the deeper zones and more specific collagen fibrils increase in diameter from the superficial to the deep layer while water content decreases. The percentage of each component in each zone can be found specifically in Table 3, [20].

Table 3. *The different morphology, size, and distribution of components in four articular cartilage zones,* [1] , [5].

Component	Superficial zone	Middle zone	Deep zone	Calcified zone
Chondrocytes				
Morphology	Flattened	Rounded	Rounded or ellipsoid	Small and inert
Collagen fibrils				
% Dry weight	86%	Between	67%	ND
Diameter	30-35 nm	Between	40-80 nm	ND
Proteoglycan				
% Dry weight	15%	25%	20%	ND
Water				
% Wet weight	84%	Between	40-60%	ND
Total thickness				
% Total tissue	10-20%	40-60%	20-30%	ND

**Data obtained from* [2] , [3] , [4], [5], [6] .

CHAPTER 2. THEORETICAL BACKGROUND

2.1 Porosity

To control the permeability of fibrous materials and generally porous materials one must consider a very important key parameter, porosity. Porosity is a non-dimensional quantity and is the percentage of space that exists in a material. It's, the volumetric fraction of the fluid that is in the pores of the medium. The symbol for porosity is the φ letter and it takes values from 0 to 1 or from 0% to 100%. The equation that describes it is the following (Fetter, 2001):

$$\varphi = \frac{V_{void}}{V_{total}} \quad (1)$$

Where φ stands for the porosity of material (%),

- V_{void}= Volume of empty space of material, (m^3)
- V_{total}= Total volume of material, (m^3)

Material's porosity can change over time and has an important correlation with permeability. It has been shown that in ordered or disordered fibrous media permeability is a strong function of porosity, as will be elaborated in subsequent sections.

2.2 Permeability

Fluid flow through a porous medium plays a significant role in many scientific and engineering applications such as tissue engineering. One of the most significant properties of porous materials is their hydraulic permeability. Although numerous studies have been conducted on this well-researched topic, the accurate determination of hydraulic permeability of fibrous media considering their complicated geometrical structures and

possible slip effect remains to be solved. In simple words, hydraulic permeability is a coefficient that measures the ability of a porous medium to be permeated by a fluid. The hydraulic permeability of a porous material depends on several parameters, such as the properties of the fluid, porosity, fibers size distribution and arrangement (in the case of fibrous porous media as will be studied in this Thesis) and of the parameters that characterize the type of transport. So, it would be right if we singled out the permeability of the material from the properties of the fluid in describing fluid flow through articular cartilage.

The permeability, *k*, describes the ease of flow via Darcy's law which was first determined experimentally by Henry Darcy (1855). Darcy's law relates the permeability of the porous medium, the viscosity of the permeating fluid as well as the pressure drop that drives the flow. The equation of Darcy's law is the following:

$$Q = (\frac{kA}{\mu L})(\Delta P) \tag{2}$$

Where,

- Q = volumetric flow rate, [m^3/s]
- A= the area of porous media normal to the flow, [m^2]
- μ= fluid's dynamic viscosity, [Pa*s]
- ΔP = pressure drop, [Pa]
- L= length in the direction of the pressure drop ΔP, [m]
- k= permeability of porous medium, [m^2]

The above model describes the flow of Newtonian fluids through porous materials and it states that the volumetric flow rate (Q) through a constant area specimen is proportional to the cross-section area (A), the pressure difference over the specimen (ΔP) and inversely proportional to the length in the direction of the specimen (L) and the viscosity (μ) [3], [21]. The aforementioned Darcy's equation was used in this study to validate the solution from the OpenFOAM software that was used. For low Reynolds number Re flows, as discussed

above, the pressure gradient over a porous medium is proportional to the fluid velocity Darcy's law.

2.2.1 Permeability in Articular Cartilage – Importance of microstructure

According to Maroudas et al. [15], permeability in AC plays a significant role as is one of the main sources of resistance to the fluid flow. The permeability of a porous medium depends strongly on its microstructure and is a macroscopic quantity that considers several microscopic phenomena, [22]. Microstructure of disordered fibrous materials, in general, can be considered to fall into three major categories: Unidirectional structures, where axes of all cylindrical fibers are parallel with one another, layered structures, where axes of cylindrical fibers lie randomly in parallel planes often perpendicular to a fluid flow, and three-dimensionally isotropic structures, where fiber axes can be randomly oriented in any direction in three- dimensional space. The magnitude of the permeability is dependent on the diameter of the fibers and the viscosity of the interstitial fluid. Since the permeability is a tensor, its principal components also depend by their configuration relative to the flow.

Flow through a poroelastic media was initially described by Biot [23]. AC as a biphasic, in the presence of load, it deforms its solid matrix and modifies the fluid hydrostatic pressure within. Many scientists studied biphasic tissues and specifically AC as biomechanical model. Mow et al. [24], studied the mechanical behavior and response of AC proposing a linear biphasic model and other researchers like Ateshian et al. [25], Hasimoto et al. [26] and Murakami et al. [27], tried to describe AC as a load bearing system with analytical solutions. However, the geometry and boundary conditions are too complicated to derive an analytic solution in such cases. Due to the complex system of equations that materials such as AC requires, many scientists have used the finite element method (FEM) for biological tissues and porous materials. Olsen [28], predicted the transient load-carriage behavior of AC using a finite element methodology. Herzog et al. [29], used the commercial FEM model ABAQUS to examine the contact problems between the layers in AC. Also, Li et al. [30], applied Finite Element hip Model method to identify the cartilage contacts and how is loaded in a hip joint and during its motion. Spilker and Suh [31], used a finite element formulation as well for articular cartilage and other hydrated

soft tissues, which consists of an incompressible, inviscid fluid phase and an incompressible solid phase.

Size of pores in tissues plays also a significant role in permeability change according to Holmes and Mow (1990) [24]. In 2020, Papathanasiou et al [32], investigated the intense effect of collagen fiber diameter distribution on hydraulic permeability in Anterior Cruciate Ligament (ACL) tissue. Recently, Zeman et al. [33] studied the impacts of the fiber arrangement, fiber diameter, and deformations of the fibers on the hydraulic permeability of fibrous membranes.

2.2.2 Analytical Models for the Permeability of Fibrous Materials

Many researchers have tried to predict the permeability of fibrous materials. Generally, the determination of permeability values is done by experimental measurements, analytical models, or Finite Element (FE) numerical simulations [34]. Sullivan started in 1940s [35] and Kuwabara [36] developed a model which predicted the permeability for flow normal to randomly arranged fibers for materials with high porosity. Happel and Brenner [37] did also theoretical analyses and they used a free surface model to solve the Stokes equation for parallel and normal flow for a single cylinder (limited boundary layer). Happel and Brenner employed different boundary conditions than Kuwabara's work. They calculated that the flow resistance of a random 3D fibrous construction equals one-third of the parallel plus two-thirds of the normal flow resistances of a 1D cylinder array. In 1950s, Hasimoto [26], Sparrow and Loeffler [38], determined the permeability of normal and parallel flow to ordered arrangement of cylinders, respectively. The same decade, Happel [39], used a free-surface model and by solving the Stokes equation for parallel and normal flow in a fibrous porous medium with a periodic array, found the permeability of fibrous porous media. In 1982, Sangani and Acrivos [40], studied the flow through 2D square and hexagonal periodic cylindrical arrays where their axes were perpendicular to the direction of the flow, and they determined the permeability of these kind of structures. Drummond and Tahir [41] solved Stokes equations for normal and parallel flow approaching various organized objects. To determine the flow-field in square, triangular, hexagonal, and rectangular arrays, they employed a distributed singularities technique. They compared their findings to Sangani

and Acrivos [40] numerical figures for normal flow. Drummond and Tahir's model for predicting transverse permeability values was extremely near to Sangani and Acrivos' model, indicating that it is only accurate for very porous materials. Brushke and Advani [42], did a more realistic approach where they considered the flow across regular cylinder arrays. For low porosities, the lubrication technique is used, while for large porosities, the analytic cell model solution is used. Both experimentally and conceptually, Tamayol and Bahrami [43], investigated the transverse permeability of fibrous porous media. The transverse permeability of fibrous media using a variety of fibrous matrices, including square, staggered, and hexagonal unidirectional fiber configurations, is determined using a scale analysis approach. Recently, using experimental data, Tomadakis and Robertson [44], stated that the upper and lower bounds for fibrous media with random orientation of fibers were normal and parallel permeability of 1D arrangements. Gebart (1992) [21], presented two models (which were used in this thesis) for the permeability for flow along and perpendicular to a perfect arrangement of fibers. He used a combination of theoretical, computational, and experimental methods and both of these models are expressed in terms of the fiber volume fraction and the fiber radius.

In 2009, Tahir and Tafreshi [45], studied the influence of in-plane and through-plane fiber orientations to a variety of fibrous structures including square, staggered, and hexagonal on a fibrous system’s transverse permeability. They developed three-dimensional virtual geometries that resemble the microstructure of fibrous media with various fiber orientations to use them in permeability calculations using numerical Stokes equations in the void space between fibers. Furthermore, their results agreed with the current experimental and analytical studies in the literature. Below we can see a plot where they studied the effect of fiber orientation on the transverse permeability of fibrous structures. They conclude that the square arrangements and 2D structures have similar permeabilities and 3D structures are the most permeable microstructure, [45]

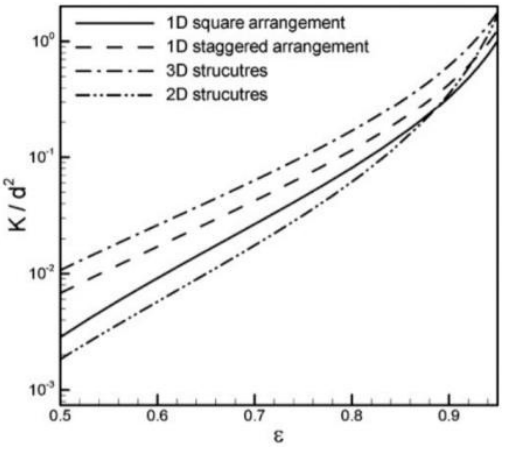

Figure 3. *Effect of fiber orientation on the permeability of fibrous structures,* [45].

To conclude, after many comparisons, concerning microscopic permeability, Gebart (hexagonal), Drummond and Tahir (hexagonal), and Kuwabara models are elected to be the most accurate models for parallel and transversal permeability, [34].

Although there are many equations and work for permeability for fibers that are parallel or tangential in 1D, 2D, 3D, there is little work on permeability calculations in three-dimensional random fiber orientations. Stylianopoulos, Yeckel, and J. Derby, et al. [46], in their work in 2008, they used the finite element method on fibers with different orientations, and combinations of results for flows parallel and perpendicular to a single fiber or an array thereof, using a volume-averaging theory, were compared to the detailed analysis, [34]. They concluded that a weighted combination of drag coefficients for spatially periodic arrays of fibers could be used as a good approximation for fiber networks, which further implies that the effect of the fiber volume fraction and orientation on the permeability of fiber networks are more important than the effect of local network structure. Also, Clague & J. Phillips in their work, calculated the hydraulic permeability of porous media comprised of three-dimensional disordered and ordered cylindrical fibers in random orientation, and in monomodal and bimodal systems, [47]. The effect of fiber bundling on permeability has been investigated by Papathanasiou and co-workers; this included the effect of bundling and its structure, including bundles of circular ([48], [49], [50], [51]) and elliptical crossections [52]. The effect of small-scale aggregation on permeability was studied in ([53], [54], [55]) and a dimensionless correlation was proposed. Methods for determining the extent of fiber alignment were proposed in [56] and the effect

of non-negligible Reynolds number was investigated in [57]. Finally, the effect of the presence of fibers of variable size were investigated in ([58], [59]).

Table 4. Permeability fibrous models

Author	**K/d²**	**Comments**
Gebart (1992)	$C(\sqrt{\frac{1-Ec}{\varepsilon}}-1)^{5/2}$ Ec = 1- π/4 Ec = 1-(π)2√3)	Square configuration: $K^{S}{}_{D}/d^2$ Hexagonal config.: K^{h}/d^2
Bruschke and Advani (1993)	$\frac{(1-l^2)^2}{12l^2}(3l\frac{tan^{-1}(\sqrt{\frac{1+l}{l}})l}{\sqrt{1-l^2}}+\frac{l^2}{2}+1)^{-1}$	Lubrication theory, square configuration of fibers: $l^2 = 4/\pi(1-\varepsilon)$
Drummond and Tahir (1984)	$\frac{1}{32\varphi}(\ln\left(\frac{1}{\varphi}\right)-1.476+\frac{2\varphi-0.796\varphi^2}{1+0.489\varphi-1.605\varphi^2})$	Square configuration: $K^{S}{}_{D}/d^2$
Drummond and Tahir (1984)	$\frac{1}{32\varphi}(\ln\left(\frac{1}{\varphi}\right)-1.476+2\varphi-\frac{\varphi^2}{2}-0.739\varphi^4+\frac{2.534\varphi^5}{1+1.2758\varphi})$	Hexagonal config.: K^{h}/d^2
Kuwabara (1959)	$\frac{1}{32\varphi}(\ln\left(\frac{1}{\varphi}\right)-1.5+2\varphi-\frac{\varphi^2}{2})$	Based on Stokes approximation
Hasimoto (1959)	$\frac{1}{32\varphi}(\ln\left(\frac{1}{\varphi}\right)-1.476)$	-
Sangani and Acrivos (1982)	$\frac{1}{32\varphi}(\ln\left(\frac{1}{\varphi}\right)-1.476+2\varphi-1.774\varphi^2+4.076\varphi^3)$	-
Happel (1959)	$\frac{1}{32\varphi}(\ln\left(\frac{1}{\varphi}\right)-\frac{1-\varphi^2}{1+\varphi^2})$	-
Lee and Yang (1997)	$\frac{\varepsilon^3(\varepsilon-0.2146)}{31(1-\varepsilon)^{1.3}}$	Valid for 0.435 < ε < 0.937 ε = porosity
Sahraoui And Kaviani (1992)	$\frac{0.0152\varepsilon^3}{1-\varepsilon}$	Valid for 0.4 < ε < 0.8 ε = porosity

2.2.3 Role of Fiber Structure in Permeability

As discussed above, permeability of fibrous media has been vastly studied for the past decades and there are many publications reporting on its variations as a function of flow regime and/or the microstructure of the fibrous medium. Many researchers have determined that the structure of the collagen fibers is thought to relate strongly to their function in the cartilage, and it has been thought that they constitute the major source of anisotropy in the elastic properties of AC (e.g., Farquhar et al., 1990; Soulhat et al., 2000; Holzapfel et al., 2000; Ogden, 2003; Federico et al., 2005; Gasser et al., 2006). But the main question that still remains unanswered is how significant is the effect of the fibers arrangement on cartilage's permeability.

Maroudas and Bullough in 1968 [60], observed that, in the superficial zone the axial permeability decreased rather than increased, due to the arrangement of the fibers and the higher collagen fibers volumetric fraction in the superficial compared to the other zones. Also, Han et al. in 2000 [61], determined the anisotropy of diffusion coefficient in tendons is due to the fact that the collagen fibers are oriented along the axis of the tendon, and restrict the mobility of water molecules more in the transverse direction (transverse to the tendon, i.e., orthogonal to the fibers) than in the axial direction (i.e., parallel to the fibers) [11]. Later in 2004, Wellen et al. [62], confirmed Han's theory for porous media. Federico and Herzog in 2007 [12], investigated the undeformed permeability of articular cartilage, by accounting for the effect produced by the collagen fibers. In their experiment they used a general model for fiber-reinforced porous materials. They found that the permeability is anisotropic and inhomogeneous as they shown in the Figure 4 below, and that it depends on the orientation of the collagen fibers.

More specific, for cartilage has been found that in the deep zone, where the fibers are aligned in the axial direction, permeability is greater in the axial than the transverse direction. Also, in the middle zone, where fibers are randomly oriented, permeability was found to be isotropic. Lastly, in the superficial zone, where the fibers lay on the transverse plane, the permeability is greater in the transverse plane than in the axial direction.

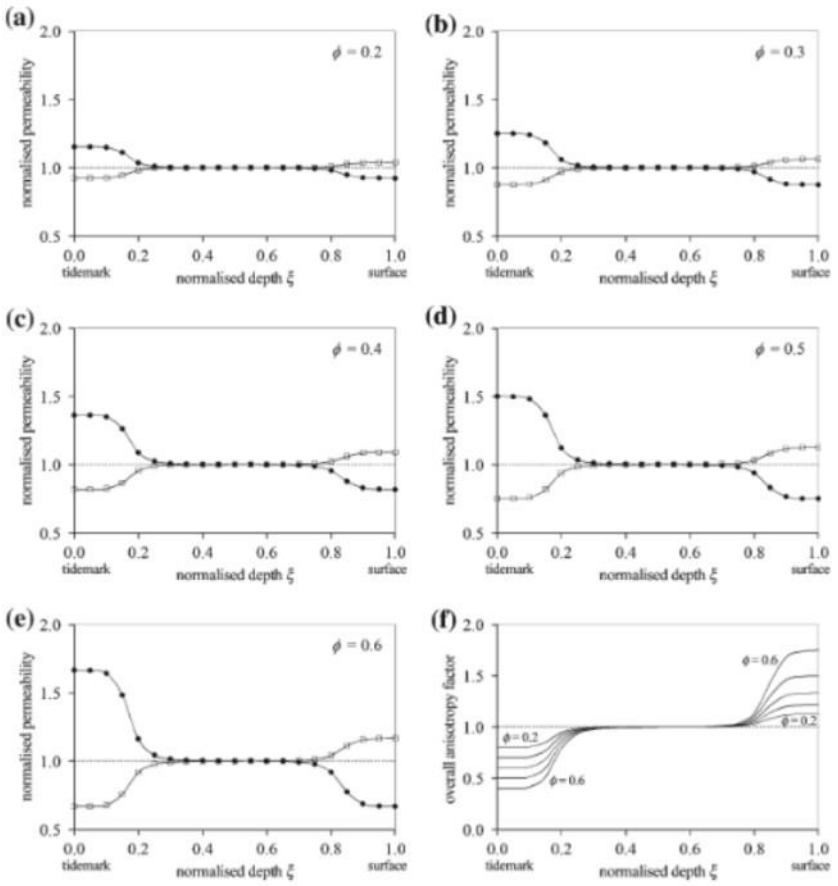

Figure 4. *Overall axial permeability (solid circles) and transverse permeability (open squares) (a–e), and overall anisotropy facto, X=K⊥/K|| (f), as a function of the normalized depth, ξ, for values of the collagen fibers volumetric fraction, φ, ranging from 0.2 to 0.6,* [62].

CHAPTER 3. COMPUTATIONAL PART

3.1 Gmsh Introduction

Christophe Geuzaine and Jean-François Remacle created Gmsh, a finite-element mesh generator. Gmsh is a three-dimensional finite element mesh generator with a CAD engine and post-processor integrated. Geometry description, meshing, solution, and post-processing are the modules that Gmsh is built around. Gmsh offers advanced visualization mechanisms and enables parametric input. Gmsh offers complete constructive solid geometry features, based on Open Cascade Technology, since version 3.0. Based on Open-Cascade Technology, Gmsh contributes to the following basic functions:

- Using geometry generation instructions to create a model.
- The discretization of a model created either in Gmsh or in another program. In 1D, 2D, and 3D models, it can create a grid.
- On the created discrete models, the solution of differential equations.
- The ability to alter the outcomes

3.2 Preprocessing Case Geometry and Mesh Generation

3.2.1 Preprocessing Case Geometry

The geometry of AC was a simple 2D rectangular shape. In essence, we «cut» the articular cartilage into a thin slice with a rectangular geometry, using real dimensions from the literature. The 2D geometry was designed and meshed in Gmsh open-source software and it is shown below in Figure 5. The geometry was created in a single plane (2D) by first constructing all points, then merging the points into lines, and finally combining the lines into a surface. Then, the final surface with the appropriate dimensions was extruded into 3D space and the boundaries of the surfaces were defined as Physical Groups and the volume of the geometry was also selected. The Extrude statement should be recombined

to have a single layer to ensure that mesh blocks are only constructed in 2D and subsequently extended to 3D, rather than being divided along the 3rd axis.

The height of the rectangle represents the thickness of AC and it was set for 2mm. Also, the length of rectangular was set for L = 5mm. Each cartilage zone had a different thickness.

More specifically,

- *Superficial zone* makes up 20% of the total cartilage thickness, T_{sup} = 0.4 mm.
- *Middle zone* makes up 50% of the total cartilage thickness, T_{middle} = 1 mm.
- *Deep zone* makes up 30% of the total cartilage thickness, T_{deep} = 0.6 mm.

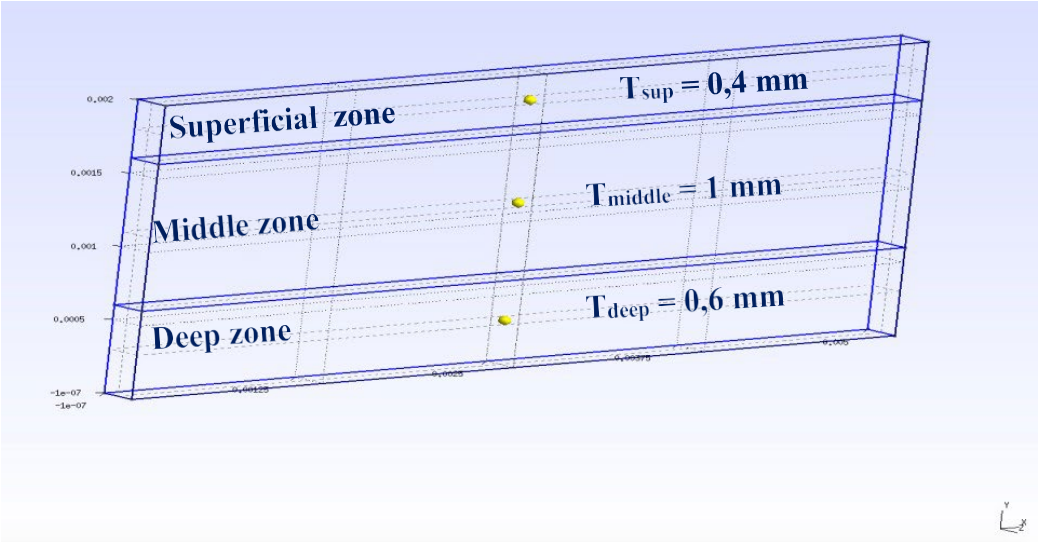

Figure 5. *2D Geometry of Articular Cartilage in Gmsh software.*

3.2.2 Mesh Generation

After creating the geometry as indicated above, the geometry meshing on which the governing equations will be solved was the next step. Mesh creates a distinct representation of the geometry. It is the task of a mesh generator as Gmsh, to create node locations and element topology so as to create high quality meshes. The mesh of the geometry was generated using the Gmsh generator. The mesh of the above geometry has the following parameters and number of cells.

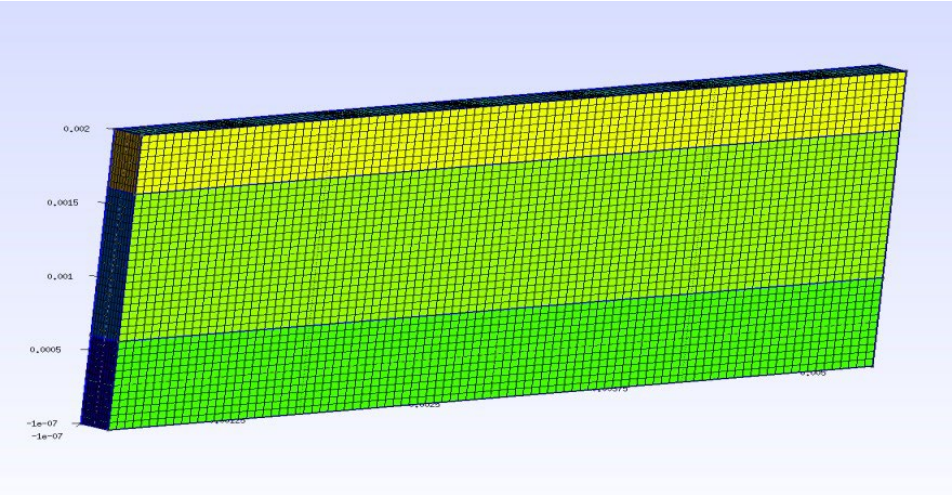

Figure 6. *2D Geometry of Articular Cartilage after being meshed in Gmsh software.*

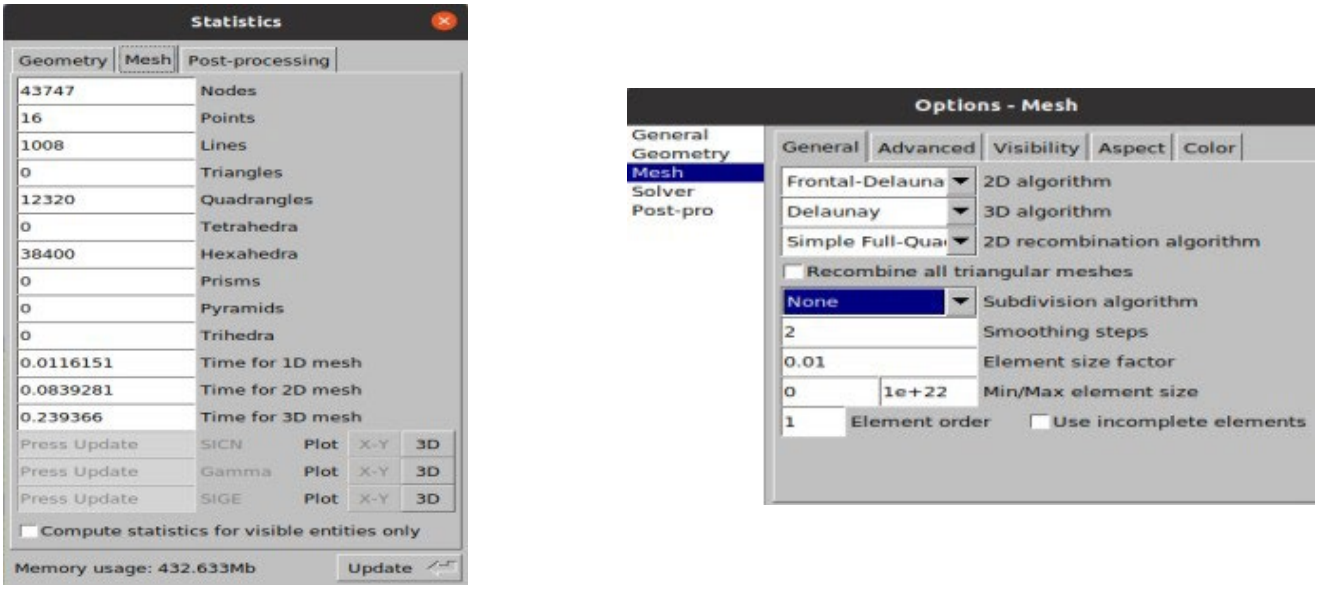

Figure 7. *Number of Cells and Mesh Properties in Gmsh software.*

3.3 OpenFOAM

3.3.1 History

OpenFOAM began as FOAM at Imperial College, London, in 1993, as a collaboration between Weller and Jasak, who was working on his PhD thesis at the time (1996). The desire to design CFD software from the ground up stemmed from unhappiness with FORTRAN scripts and the desire to produce something that could be reused by others. FOAM was developed as closed-source commercial software for a few years before becoming open source in December 2004 with the release of OpenFOAM 1.0. Six major releases have been released since then. Many R&D teams in academic institutions and industry use OpenFOAM.

3.3.2 Introduction to OpenFOAM

OpenFOAM which stands for “Open-Source Field Operation and Manipulation" is first and foremost a C++ library, used primarily to generate executables, known as applications. OpenFOAM includes a wide range of capabilities that can be used to address a wide range of problems, including chemical processes, turbulence, and heat transport, as well as solid dynamics and electromagnetics. There are two types of applications: solvers, which are meant to solve a specific problem in continuum mechanics, and utilities, which are designed to execute data manipulation tasks. Numerous solvers and utilities are included in the OpenFOAM package, which cover a wide spectrum of issues. One of OpenFOAM's advantages is that users can construct new solvers and utilities with some prior knowledge of the underlying approach, physics, and programming techniques. Pre- and post-processing environments are included in OpenFOAM. The pre- and post-processing interfaces are all OpenFOAM utilities, guaranteeing that data is handled consistently across all contexts. The overall structure of OpenFOAM is shown in Figure 8.

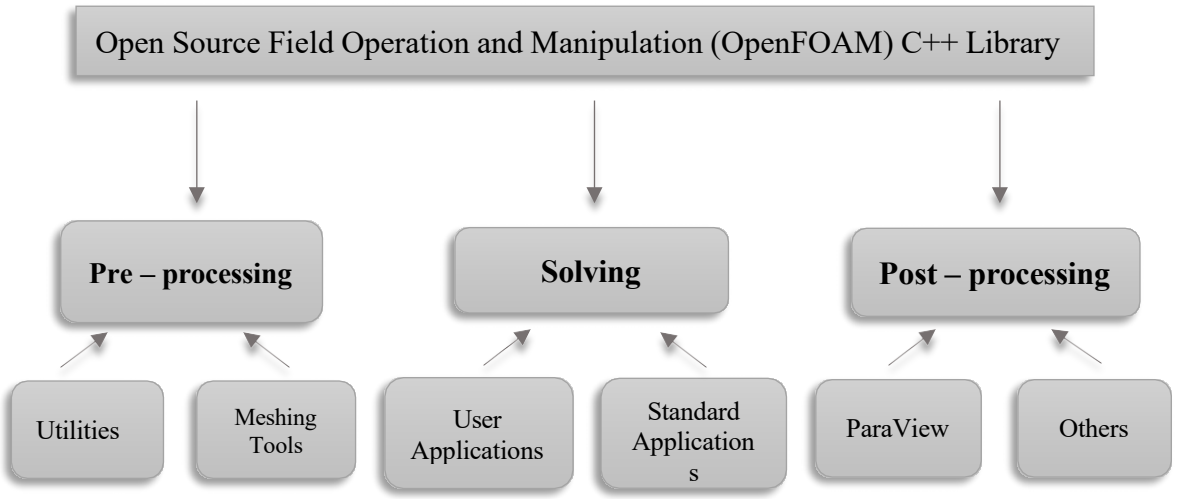

Figure 8. *Overview of OpenFOAM structure.*

OpenFOAM has tutorials and instructions that contain many cases that demonstrate the use of all the solvers and supplied many utilities. The tutorial cases describe the use of the blockMesh pre-processing tool, case setup and running OpenFOAM solvers and post-processing using ParaView. ParaView is an open source multiple platform application, designed for interactive data analysis by means of qualitative and quantitative techniques and all the scientific data sets can be visualized there. OpenFOAM does not have a generic solver applicable to all cases. Instead, users must choose a specific solver for a class of problems to solve and OpenFOAM can solve a plethora of problems of different scientific fields.

3.3.3 Standard Solvers

OpenFOAM is primarily a tool for solving partial differential equations, rather than a standard CFD software and over 80 solver applications are included in it. Solvers are further subdivided into numerous subdirectories based on the continuum mechanics category, such as incompressible flow, heat transfer, multiphase, lagrangian, and combustion. Below in Figure 9 a list of available *incompressible* solvers is presented.

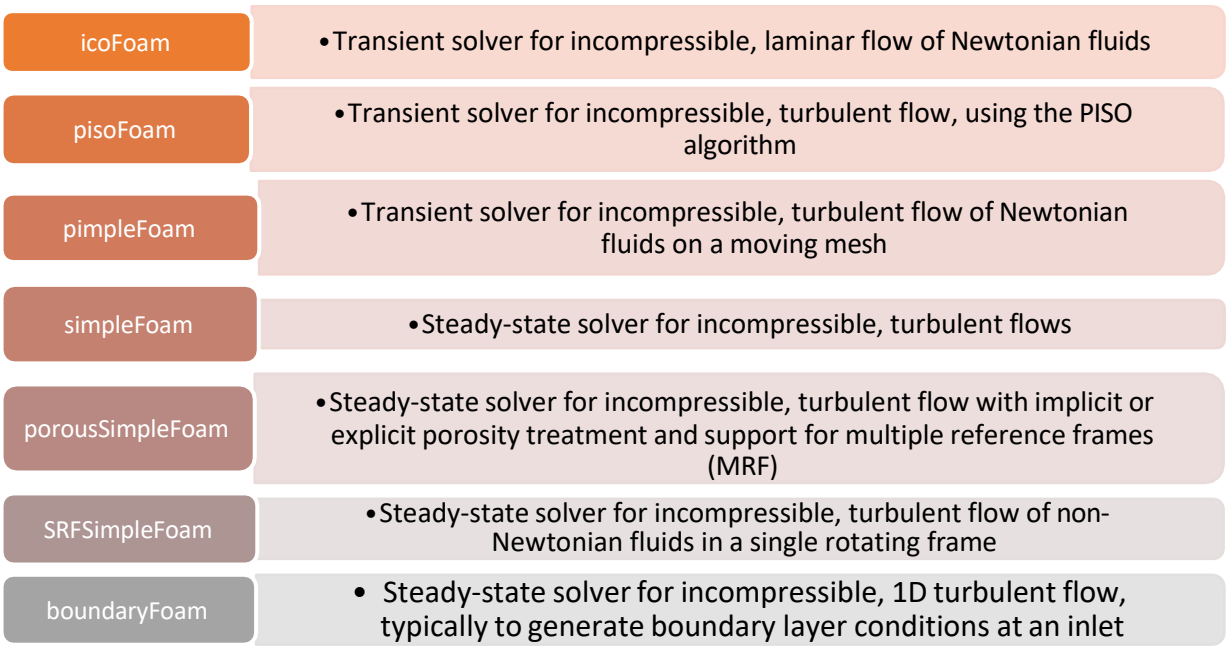

Figure 9. *Basic incompressible OpenFOAM solvers.*

3.3.4 Case set up

Every OpenFOAM case has a similar structure, with minor changes arising solely from the solver used. The basic file structure corresponds to that of Figure 10. All files in black text are required files to set-up a working case for each solver.

The following are the steps to follow while starting up a simulation in OpenFOAM: The boundary conditions must be set, the fluid characteristics must be chosen, the numerical schemes and algorithms for solving systems of equations must be chosen, and the general simulation settings must be finalized. More precisely,

- ***«constant directory»:*** It contains a full description of the case mesh in a subdirectory «polyMesh» and files specifying physical properties for the application concerned, e.g. transport Properties.
- ***«system directory»:*** For setting parameters associated with the solution procedure itself. It contains at least the following three files:

- ***«controlDict»*** where run control parameters are set including start/end time, time step and parameters for data output. The OpenFOAM solvers begin all runs by setting up a database. The database controls I/O and, since output of data is usually requested at intervals of time during the run, time is an inextricable part of the database.
- ***«fvSchemes»*** where discretization schemes used in the solution may be selected at run-time; Here we set the numerical schemes for terms, such as derivatives in equations, that are calculated during a simulation. "The terms that must typically be assigned a numerical scheme in fvSchemes range from derivatives, e.g. gradient ∇, to interpolations of values from one set of points to another. The aim in OpenFOAM is to offer an unrestricted choice to the user, starting with the choice of discretization practice which is generally standard Gaussian finite volume integration. Gaussian integration is based on summing values on cell faces, which must be interpolated from cell centers. The user has a wide range of options for interpolation scheme, with certain schemes being specifically designed for derivative terms, especially the advection divergence ∇· terms
- ***«fvSolution»*** where the equation solvers, tolerances, and other algorithm controls are set for the run. It's in this file that the solvers, algorithms, and under-relaxation factors are set. If any parameter or sub dictionary is missing when a solver is run, it will terminate, printing a detailed error message.

- ***«time directories»:*** They contain individual files of data for particular fields. The data can be either initial or boundary values that the user must specify to define the problem or results written to file by OpenFOAM.

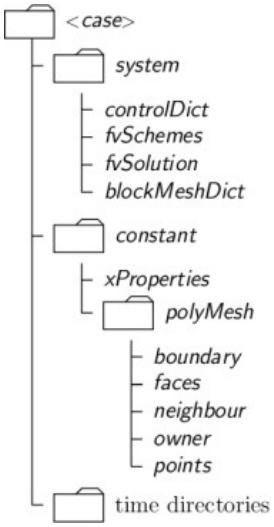

Figure 10. *Case directory structure for OpenFOAM.*

3.3.5 Boundary Conditions

After the geometry of the problem has been defined and the mesh has been generated, boundaries conditions of the problem must be provided. This step takes place within the blockMeshDict file of the case directory in OpenFOAM. For the current case geometry, 6 boundary sets, or patches, needed to be specified, namely:

- *right*: The boundary where the flow exits from AC.
- *left:* Symmetry to the right face of the AC.
- *top*: The top boundary of AC.
- *bottom*: The bottom boundary of AC.
- *front*: The front side of the AC.
- *back*: the back side of the AC.

The special variable values for the aforementioned boundary sets/patches are given in the *0* folder. The case is set up to start at time t = 0 sec, so the initial field data is stored in a *0* sub-directory. For an incompressible flow, 0 sub-directory contains 2 files, *P* and *U*, one for each of the pressure and velocity fields whose initial values and boundary conditions must be set. The dimension of the variable is allocated through dimensions in the folder (for instance m/s for the velocity). The internal field is set through internalField and the

boundary field is given through boundaryField. There are 3 principal entries in field data files. In detail,

- ***Dimensions:*** specifies the dimensions of the field.
- ***InternalField:*** the internal field data which can be uniform, described by a single value; or nonuniform, where all the values of the field must be specified. In the current case internalField is uniform as is shown in Figure 8.
- ***BoundaryField:*** the boundary field data that includes boundary conditions and data for all the boundary patches. In this case we have 3 different entry conditions:

  - ***fixedValue:*** This boundary condition provides a fixed value constraint and serves as the foundation for several other boundary conditions.
  - ***zeroGradient:*** This boundary condition imposes a zero-gradient constraint on the patch faces from the patch internal field.
  - ***empty****:* For reduced dimensions scenarios, such as 1-D and 2-D geometries, this boundary condition gives an 'empty' condition. This condition should be applied to patches whose normals are aligned with geometric directions that aren't solution directions.

The pressure and velocity boundary conditions used in this study are represented in the figures below. At the top surface of AC where is the superficial zone a displacement in -y direction was set. At the right face where there is the outflow of the fluid the boundary condition was set as *zeroGradient*. In the bottom patch where is the bone of the knee joint there is no velocity, so the boundary condition was set as a *fixedValue* of 0 m/s. For the pressure conditions of the case, *zeroGradient* boundary was set for the top, bottom, and left patch of the geometry due to the free flow of these surfaces. The pressure of the right surface was set as zero.

```
/*--------------------------------*- C++ -*----------------------------------*\
  =========                 |
  \\      /  F ield         | OpenFOAM: The Open Source CFD Toolbox
   \\    /   O peration     | Website:  https://openfoam.org
    \\  /    A nd           | Version:  8
     \\/     M anipulation  |
\*---------------------------------------------------------------------------*/
FoamFile
{
    version     2.0;
    format      ascii;
    class       volVectorField;
    object      U;
}
// * * * * * * * * * * * * * * * * * * * * * * * * * * * * * * * * * * * * *

dimensions      [0 1 -1 0 0 0 0];

internalField   uniform (0 0 0);

boundaryField
{
    top
    {
        type            fixedValue;
        value           uniform (0 -0.001 0);
    }

    bottom
    {
        type            fixedValue;
        value           uniform (0 0 0);
    }

    right
    {
        type            zeroGradient;
    }

    front
    {
        type            empty;
    }

    left
    {
        type            zeroGradient;
    }

    back
    {
        type            empty;
    }
}

// ************************************************************************* //
```

```
/*--------------------------------*- C++ -*----------------------------------*\
  =========                 |
  \\      /  F ield         | OpenFOAM: The Open Source CFD Toolbox
   \\    /   O peration     | Website:  https://openfoam.org
    \\  /    A nd           | Version:  8
     \\/     M anipulation  |
\*---------------------------------------------------------------------------*/
FoamFile
{
    version     2.0;
    format      ascii;
    class       volScalarField;
    object      p;
}
// * * * * * * * * * * * * * * * * * * * * * * * * * * * * * * * * * * * * *

dimensions      [0 2 -2 0 0 0 0];

internalField   uniform 0;

boundaryField
{
    top
    {
        type            zeroGradient;
    }

    bottom
    {
        type            zeroGradient;
    }

    right
    {
        type            fixedValue;
        value           uniform 0;
    }
    front
    {
        type            empty;


    }
   left
    {
        type            zeroGradient;
    }

    back
    {
        type            empty;

    }
}

// ************************************************************************* //
```

Figure 11. *Boundary Conditions for Velocity (left) and Pressure (right).*

3.3.6 Physical Properties

The physical properties of a fluid, also known as mechanical properties, play a crucial role in the field of fluid mechanics, as they determine aspects of the flow behavior. In an OpenFOAM case, the physical properties of fluids are defined in the *transportProperties* file. In the science of fluid mechanics, a fluid's physical properties, also known as mechanical properties, are critical because they govern aspects of flow behavior. The physical properties of fluids are defined in the *transportProperties* file in an OpenFOAM case set up. For a PorousSimpleFoam case, the only property that must be specified is the kinematic viscosity which is stored in *transportProperties*. Initially this case will be run with a Reynolds number of 50, where the Reynolds number is defined as:

$$Re = \frac{L\,|U|}{v} \tag{3}$$

Where,

- L = the characteristic length (m)
- $|U|$ = the characteristic velocity (m/s)
- v = the kinematic viscosity (m^2/s)

The Reynolds number, referred to as Re, is used to determine whether the fluid flow is laminar or turbulent. Flows with low Reynolds numbers tend to be laminar, while those with high Reynolds numbers tend to be turbulent. In this research we have an incompressible laminar flow and for this reason turbulence model was turned off as is shown in *momentumTransport* folder (Figure 13).

Figure 12. *TransportProperties file in directory.*

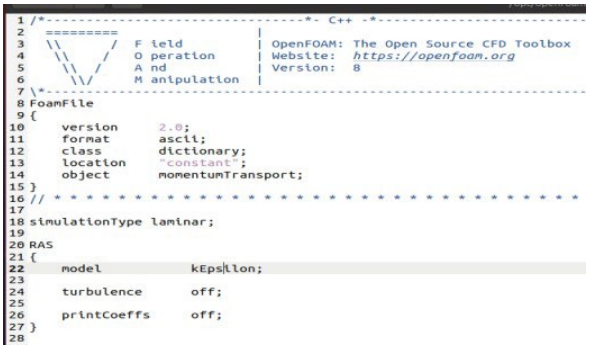

Figure 13. *MomentumTransport properties file in directory.*

The units of measurement for each quantity are stated in addition to the parameter values. This works by combining seven basics S.I. measuring units, which are listed in brackets before each amount value. Each number represents the measurement unit's power setting. Table 5 shows the relationship between the units and bracket positions:

Table 5. *Correspondence between the units and the bracket positions.*

Bracket Position	Quantity	Measurement Unit
1	Mass	Kg
2	Length	M
3	Time	Sec
4	Temperature	K
5	Amount of Substance	Mol
6	Electric Current	A
7	Luminous Intensity	Cd

3.3.7 Control

The execution of flow simulations needs the input of time and general output control data. The *controlDict* dictionary contains these as well as other details about the resulting solution. The solver's start and end times, as well as the timestep, are set in *subdictionaries* within the file. These figures do not apply to all cases, but rather vary from one to the next. *ControlDict* specifies essential output information in addition to time control. These mostly consist of instructions for recording and storing the results.

```
/*--------------------------------*- C++
  =========                 |
  \\      /  F ield         | OpenFOAM: T
   \\    /   O peration     | Website:  h
    \\  /    A nd           | Version:  8
     \\/     M anipulation  |
\*---------------------------------------
FoamFile
{
    version     2.0;
    format      ascii;
    class       dictionary;
    location    "system";
    object      controlDict;
}
// * * * * * * * * * * * * * * * * * * *

application     porousSimpleFoam;

startFrom       startTime;

startTime       0;

stopAt          endTime;

endTime         1000000;

deltaT          1;

writeControl    timeStep;

writeInterval   500;

purgeWrite      0;

writeFormat     binary;

writePrecision  6;

writeCompression off;

timeFormat      general;

timePrecision   6;

graphFormat     raw;

runTimeModifiable true;
```

Figure 14. *ControlDict file from OpenFOAM.*

3.3.8 PorousSimpleFoam solver

The porousSimpleFoam solver is the *simpleFoam* single-phase, steady-state solver for turbulent flow of incompressible fluids with implicit or explicit porosity treatment. It is based on the *simpleFoam* solver, with the porosity zones and Multiple Reference Frame (MRF) capabilities included by default in its default configuration, eliminating the need to include it in a *fvOptions* file. It also allows for the selection of an explicit or implicit porosity treatment. Porous models are commonly applied to a defined cell zone in which the momentum equation gets a new sink/source term (Darcy Forchheimer equation). Darcy Forchheimer equation is an empirical equation, which relates the pressure loss due to friction across a porous medium, with respect to the velocity of the flow inside the porous medium. So, the Darcy Forchheimer model that is added, allows the solver to simply add a porosity zone. The Navier-Stokes equations are modified to account for porous media by attenuating the time derivative and introducing a sink element Si. Considering the momentum equation, it follows:

$$\frac{\partial}{\partial t}(\rho u_i) + u_j \frac{\partial}{\partial xj}(\rho u_i) = -\frac{\partial}{\partial x_j} + \mu \frac{\partial \tau_{ij}}{\partial x_j} + S_i \quad (4)$$

Where,

- ρ = density [kg/m^3]
- u = velocity vector [m/s]
- μ = dynamic viscosity [Pa·s = kg/(s·m)]
- τ = shear stress tensor [N/m^2]

The source term, Si accounts for the Darcy Forchheimer equation and is made up of two parts: a viscous loss term and an inertial loss term, producing a pressure decrease proportional to velocity and velocity squared. F is a quadratic resistance coefficient (Forchheimer coefficient) and D is a linear resistance coefficient (Darcy coefficient) that specifies the viscous resistance and equals with the proportional of permeability K.

$$Si = -(\mu Dij + \frac{1}{2}\rho\, |ukk| Fij)\, ui \quad (5)$$

The source term Si is composed of two parts, a viscous loss term and an inertial loss term, creating a pressure drop that is proportional to the velocity and velocity squared, respectively. There are three different modes that can be used:

- Linear velocity-pressure drop relation (F = 0, only Darcy contribution)
- Parabolic velocity-pressure drop relation (D = 0, only Forchheimer contribution)
- A mixed formulation of both.

This equation is being known as the Darcy-Forchheimer equation. In the case of simple homogeneous porous medium, it becomes as below (where there is no scalar F, only Darcy contribution):

$$Si = -(\mu D)u_i \tag{6}$$

The source code for the porousSimpleFoam solver may be found in the *simpleFoam* solver directory at $FOAM APP/solvers/incompressible/simpleFoam/. Figure 15 shows the directory tree.

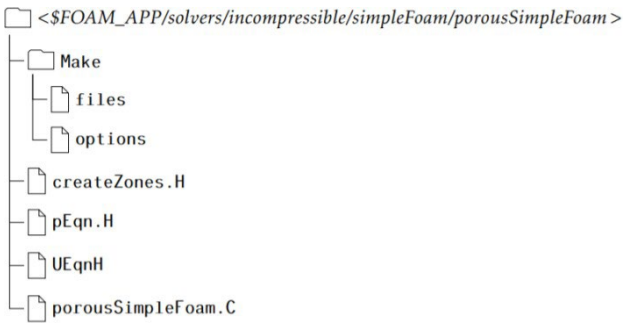

Figure 15. *PorousSimpleFoam source code folder structure.*

To employ porous zones in porousSimpleFoam, the zones in the mesh that will be treated with porosity must be first specified. The porosity properties are then defined in the file *constant/porosityProperties*.

In this step permeability of the porous material is also determined and it will be declared whether the porosity will be extended in all three directions.

```
(
    porosity
    {
        coordinateSystem
        {
            e1  (0.70710678 0.70710678 0);
            e2  (0 0 1);
        }

        Darcy
        {
            d   d [0 -2 0 0 0 0 0] (5e7 -1000 -1000);
            f   f [0 -1 0 0 0 0 0] (0 0 0);
        }
    }
)
```

Figure 16. *Porosity properties example in porousSimpleFoam.*

Porous media is added to a certain cell zone belonging to the mesh. In Figure 16 the name of the cell zone is porosity and it refers to the cell zone that is defined in the *constant/polyMesh/blockMeshDict* file. A local coordinate system can be created within the cell zone. The geometry's global coordinate system is set by default. The *coordinateSystem* class is used to be defined by the coordinate system. In Figure 16 its specified with two vectors, e1 and e2. The rectangular is aligned with the vector e1, which is formed as a linear combination of the global x- and y-axes, and the vector e2 is set orthogonal to e1. The *coordinateSystem* class then creates the vector e3 in right-hand order, orthogonal to both e1 and e2. This vector's coordinates relate to the local coordinate system. D has a default value of zero. At least one of the vector's components must be greater than zero. Negative values will be multiplied by the greatest component of the vector, and the sign will be changed to positive. The method *adjustNegativeResistance*, which is implemented in *porousZone.C*, is used to accomplish this.

3.4 Validation of PorousSimpleFoam solver

In this section, we evaluate the results of the porousSimpleFoam solver that we used in our simulations in OpenFOAM software with an analytical solution of the problem. We assumed that we have only one zone and that is isotropic with a constant permeability. Below we analyze each method respectively and we compare their results.

3.4.1 Analytical solution

Mass conservation

The mass conservation equation (or continuity equation) ensures that the net change of mass within a continuum is zero, he conservation of mass for a free flow system is defined as follows:

$$\frac{\partial \rho}{\partial t} + \nabla \cdot (\rho u) = 0 \tag{7}$$

Where *u* is the fluid velocity vector, *t* represents time, and *ρ* is the fluid density. The first term on the left side is the density's rate of change over time (mass per unit volume). The second term, known as the “convective term”, depicts the net movement of mass out of the element across its boundaries.

Taking into the account the nature of the flow studied in this thesis, i.e., that of an incompressible fluid, steady state flow, a rigid porous medium and no source or sink, Equation (7) is reduced to:

$$\nabla \overline{U} = 0 \tag{8}$$

In our case we have a 2D rectangle that represents Articular Cartilage as an isotropic porous medium. To study the pressure profile of this case we will use Continuity Equation for cartesian coordinates and the Equation (8) will take the following form:

$$\frac{dUx}{dx} + \frac{dUy}{dy} = 0 \tag{9}$$

As it has been mentioned Darcy’s Law is the first mathematical expression of fluid flow through a porous medium. For this case Darcy’s Law is used for a 2D porous medium with flow in x-direction and its form is simplified as following:

$$q = -\frac{KA}{\mu}\frac{dP}{dx} \tag{10}$$

Where, *(∂p/∂x)* is the potential gradient in x direction, μ is the fluid viscosity, and K permeability constant.

$$\frac{\mathrm{q}}{\mathrm{A}} = -\frac{\mathrm{k}}{\mu}\frac{\mathrm{dP}}{\mathrm{dx}} \tag{11}$$

$$\mathrm{U} = -\frac{\mathrm{k}}{\mu}\frac{\mathrm{dP}}{\mathrm{dx}} \tag{12}$$

From (9), (12)

$$-\frac{\mathrm{K}}{\mu}\frac{\mathrm{d}^2\mathrm{P}}{\mathrm{dx}^2} + \frac{\mathrm{dUy}}{\mathrm{dy}} = 0 \tag{13}$$

After the integration of Equation (13) in y – axis:

$$\int_0^{\mathrm{y}} \left(-\frac{\mathrm{k}}{\mu}\frac{\mathrm{d}^2\mathrm{P}}{\mathrm{dx}^2}\right) \mathrm{dy} + \int_0^{\mathrm{y}} \left(\frac{\mathrm{dUy}}{\mathrm{dy}}\right) \mathrm{dy} = 0 \tag{14}$$

And for y = H the Equation (14) will be the following:

$$-\frac{\mathrm{KH}}{\mu}\frac{\mathrm{d}^2\mathrm{P}}{\mathrm{dx}^2} + \mathrm{Uy(H)} - \mathrm{Uy(0)} = 0 \tag{15}$$

$$-\frac{\mathrm{KH}}{\mu}\frac{\mathrm{d}^2\mathrm{P}}{\mathrm{dx}^2} - \mathrm{U} = 0 \tag{16}$$

$$\frac{\mathrm{d}^2\mathrm{P}}{\mathrm{dx}^2} = -\frac{\mathrm{U}\mu}{\mathrm{KH}} \tag{17}$$

The boundary conditions for the problem are: $\frac{dP}{dx}(x = 0) = 0$ and $P(x = L) = 0$

Using the above boundaries conditions in Equation (17), we end up with the following final

equation for the Pressure profile of the problem:

$$\boldsymbol{P(x) = -\frac{\mu U}{2KH}(x^2 - L^2)} \quad (18)$$

Where,

- P = the pressure in [m^2/s^2]
- x = the horizontal axis distance [m]
- μ = viscosity in [m^2/s]
- U = velocity the upper plate moves in [m/s]
- L = horizontal length in [m]
- H = vertical distance between the plates [m]
- K = the permeability [m^2]

3.4.2 Numerical Solution

Porous media is modeled by neglecting the time derivative and by adding a sink term to the Navier-Stokes equations.

$$\frac{\partial}{\partial t}(\gamma \rho u_i) + u_j \frac{\partial}{\partial x_j}(\rho u_i) = \frac{\partial p}{\partial x_i} + \mu \frac{\partial \tau_{ij}}{\partial x_j} + S_i \quad (19)$$

The value of γ should be between 0 and 1, where the latter is a complete porosity.

$$\mathrm{Si} = -(\mu \mathrm{Dij} + \frac{1}{2}\rho|\mathrm{ukk}|\mathrm{Fij})\,\mathrm{ui} \quad (20)$$

This equation is known as the Darcy-Forchheimer equation. In the case of simple homogeneous porous media as we study here in our validation case the above Equation becomes:

$$\mathrm{Si} = -(\mu \mathrm{D} + \frac{1}{2}\rho|\mathrm{ujj}|\mathrm{F})\,\mathrm{ui} \tag{21}$$

where Dij and Fij are represented as the coefficients that have been mentioned previously.

3.5 Permeability Models used In Thesis

Gebart's and Clague's et al. [45] models have been one the most accurate models for permeability along and transversal to the fibers and in random orientation respectively. In this Chapter we will analyze the above models extensively as we used them in our computational part to calculate the permeability values of our case.

3.5.1 Gebart Model for Permeability

Gebart [45], calculated a permeability model for an isotropic fibrous porous medium which was consisted of parallel and vertically fibers. The fibers were organized in a regular pattern so that the flow could be analyzed in a single representative cell. A quadratic array and a hexagonal array were among the patterns he investigated. If the two permeabilities of a porous medium are equal, the porous medium is called isotropic; and if they are different, the porous material is called anisotropic. Below we can see the two patterns that Gebart considered as a "representative cell".

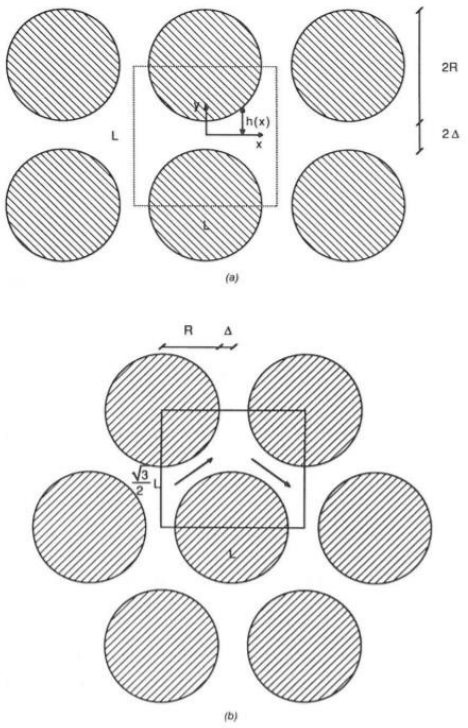

Figure 17. *Definition sketch for representative cell in a.) quadratic pattern and in b.) hexagonal pattern.*

Afterwards he introduced a tensor permeability (*K*) so the model can be applied to an anisotropic fibrous porous medium too. The permeability tensor can be used to explain the permeability of porous media in general. Depending on the coordinate system used, it is a symmetrical and positive definite second order tensor. When the chosen coordinate axes are along to the principal directions, the tensor is diagonal. In this study Cartesian coordinates are applied and the permeability tensor of AC in each zone has the following form:

$$K = \begin{Bmatrix} K_{xx} & & \\ & K_{yy} & \\ & & K_{zz} \end{Bmatrix}$$

3.5.1.1 Gebart's Model for Permeability for Flow Parallel to Fibers.

The permeability for flow along the fibers can be identified from the Equation below. Constant c depends on the array that we have. For quadratic array c takes the value of 57 and for hexagonal array c takes the value of 53.

$$K_{parallel} = \frac{8R^2}{c}\frac{(1-V_f)^3}{{V_f}^2} \quad (22)$$

Where,

- R = radius of the fibers [m]
- V_f = Volume fraction of the fibers
- c = constant

3.5.1.2 Gebart's Model for permeability for flow Perpendicular to Fibers.

The permeability for flow along the fibers can be identified from the Equation below. Parameters C_1 and Vfmax depends on if we have a quadratic pattern or a hexagonal. In Table 6 we can see the specific values of the constant parameters that we mentioned in both Equations.

$$K_{transversal} = C1\left(\sqrt{\frac{V_{fmax}}{V_f}} - 1\right)^{\frac{5}{2}} \quad (23)$$

Where,

- C_1, V_{fmax} = parameter that depends on the arrangement of the fibers
- V_f = Volume fraction of the fibers

Table 6. *Numerical Values of the parameters in Equations (22) and (23), [11].*

Fiber Arrangement	C_1	$V_{f_{max}}$	c
Quadratic	$\frac{16}{9\pi\sqrt{2}}$	$\frac{\pi}{4}$	57
Hexagonal	$\frac{16}{9\pi\sqrt{6}}$	$\frac{\pi}{2\sqrt{3}}$	53

In this thesis, the above equations of Gebart & Clague et. Al. were used for hexagonal array of fibers as AC was simulated as an anisotropic porous medium. As it has been mentioned before, AC has 3 zones with different fiber orientation is each zone, thus cartilage is an anisotropic medium and we used the permeability tensor Kxy for each zone.

3.5.2 Clague & J. Phillips Model for Permeability

Clague & J. Phillips in their work, calculated the hydraulic permeability of porous media comprised of three-dimensional disordered and ordered cylindrical fibers in random orientation, and in monomodal and bimodal systems [14]. The equation they calculated and used in their work is the following:

$$\frac{1}{K} = \frac{1}{K_p(\frac{\varphi}{3})} + \frac{1}{K_t(\frac{2\varphi}{3})} \tag{24}$$

Where,

- K_p = the permeability for flow parallel to fibers
- K_t = the permeability for transverse flow normal to the fibers

K_p is calculated by using Equation from Drummond and Tahir [15] at a volume fraction *φ/3*, and *Kt* is calculated by using Equation from Sangani and Acrivos [16] at a volume fraction *2φ/3*. The direct calculations were performed, using the finite element method, on networks with varying degrees of orientation.

3.5.3 Permeability Tensor in Each Zone

In superficial zone, fibers are parallel in the x direction. For flow in x direction permeability is parallel to the fibers. For flow in the y direction permeability is perpendicular to the fibers and in z direction permeability is also perpendicular to the fibers. As a result, the permeability tensor for this zone follows the following structure:

$$K_{sup} = \begin{Bmatrix} K_p & & \\ & K_t & \\ & & K_t \end{Bmatrix}$$

Where,

- K_p = permeability for flow parallel to the fibers
- K_t = permeability for flow tangential to the fibers

In middle zone, fibers are randomly oriented. In each direction we assume randomly permeability. As a result, middle zone can be described as an isotropic zone and the permeability tensor for this zone is the following in the three directions x, y, z:

$$K_{middle} = \begin{Bmatrix} Kr & & \\ & Kr & \\ & & Kr \end{Bmatrix}$$

Where,

- K_r = permeability for flow in randomly orientation to the fibers

At last, in the deep zone of AC the fibers are vertically in the y direction. Therefore, for flow in the x and z direction permeability is perpendicular to the fibers and for flow in y direction permeability is parallel to the fibers. Consequently, the following is the zone's permeability tensor in the three directions x, y, z:

$$K_{deep} = \begin{Bmatrix} Kt & & \\ & K & \\ & & Kt \end{Bmatrix}$$

CHAPTER 4. RESULTS

This chapter is devoted to the presentation and analysis of the results of this study. Initially the cases are formulated, and the parameters are defined. Following that, the number of cells is established through the mesh refinement process and the results are categorized, presented, and analyzed.

4.1 Validation Results

In this section, the results of the comparison between the Analytical solution from the equations that have been evaluated in 3.4.1 Chapter, and the Numerical solution that have been produced from the simulation with porousSimpleFoam solver in OpenFoam for an isotropic porous medium are presented.

For the isotropic porous medium the following properties for the problem in Table 7 have been used. More specific the velocity of the upper surface of the rectangle was set for -0.01 m/s in y direction and the height of the rectangle that represents the thickness of the cartilage was set for 2mm.

Table 7. *Parameters in validation case.*

Properties	Value	Units
Viscosity	0.000001	m^2/s
Velocity	-0.01	m/s
Permeability	2.681E-16	m^2
Vertical Distance	0.0002	m
Length	0.0005	m

Three comparisons were made changing the length (L) of the rectangular as is shown in the following Figures. What has been observed from the results, is that the analytical solution that have been obtained above matches with the results from porousSimpleFoam solver and converges perfectly for length L = 0.005m. As a result,

porousSimpleFoam solver is an accurate solver and L = 0.005m is an ideal length for the rectangular to simulate AC.

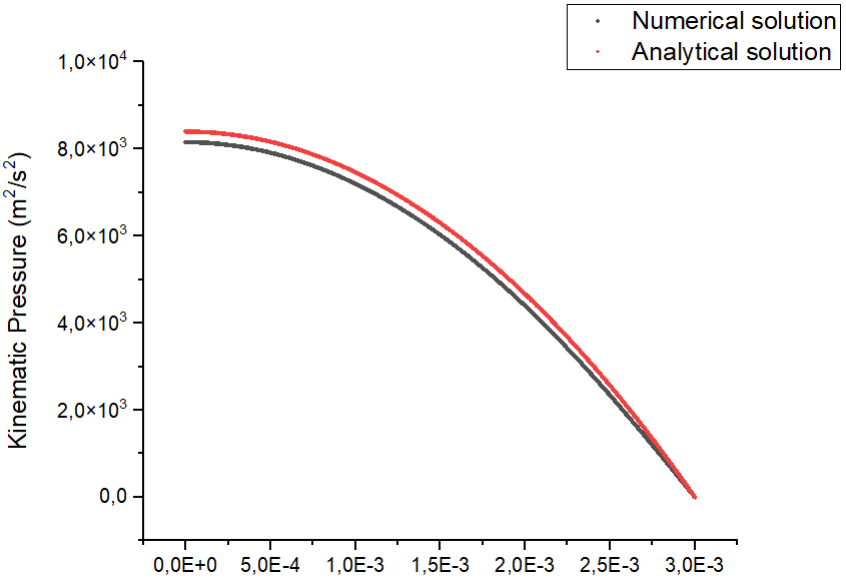

Figure 18. *Validation results for L=0.003m.*

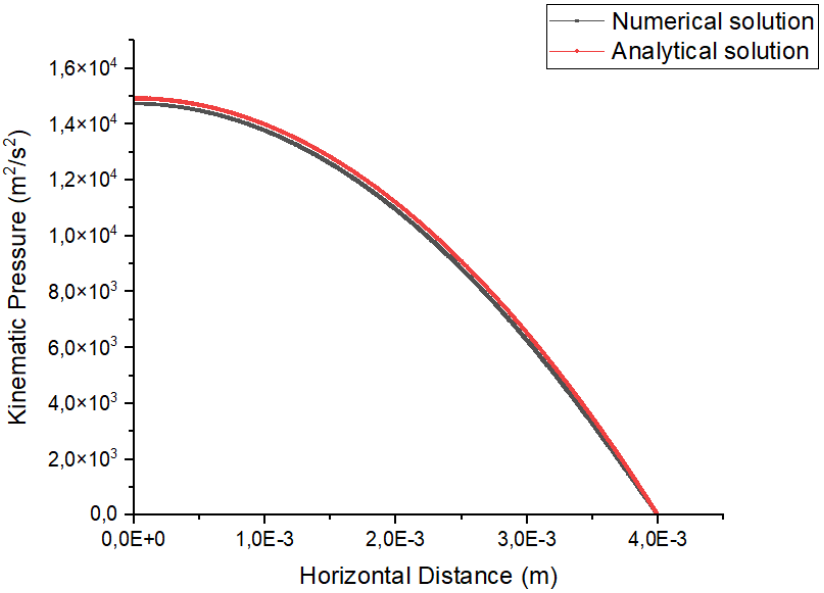

Figure 19. *Validation results for L=0.004m.*

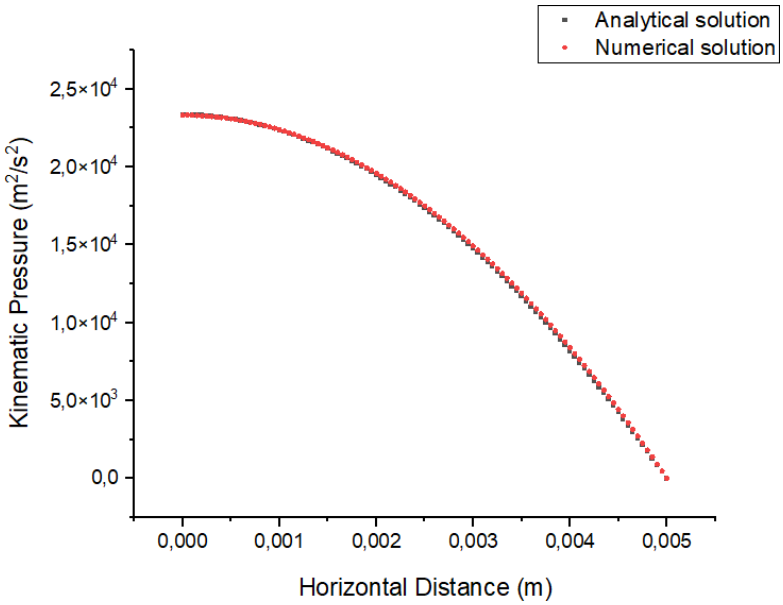

Figure 20. *Validation results for L=0.005m.*

4.2 Initially Case

The aim of this case was to simulate the three porous zones of AC in OpenFOAM software and study the pressure and velocity profiles. The following are the settings that were set for this experiment:

4.2.1 Permeability Values

As have been mentioned before, AC has different fiber orientations in each zone and as a result permeability is anisotropy. According to Chapter 2 and the permeability models that were used (Gebart and Clague & J. Phillips models), permeability in the main simulation of this research had the above values in each porous zone. In order to calculate these values, we used literature for the volume fraction and the radius of the fibers in each zone.

$$K_{sup} = \begin{Bmatrix} 1{,}5e\text{-}15 \\ & 2{,}68e\text{-}16 \\ & & 2{,}68e\text{-}16 \end{Bmatrix} \quad K_{middle} = \begin{Bmatrix} 2{,}64e\text{-}15 \\ & 2{,}64e\text{-}15 \\ & & 2{,}64e\text{-}15 \end{Bmatrix} \quad K_{deep} = \begin{Bmatrix} 1{,}31e\text{-}16 \\ & 6{,}34e\text{-}16 \\ & & 1{,}31e\text{-}16 \end{Bmatrix}$$

Figure 20. *Permeability values for initial case.*

4.2.2 Results of Pressure Profile

ParaView was used for the post-processing and the visualizing of the results from the calculations made by OpenFOAM in the simulation. The case files and results can be seen in the software ParaView or any other post-processing application once the chosen solution has reached the maximum time steps and the case has been recreated.

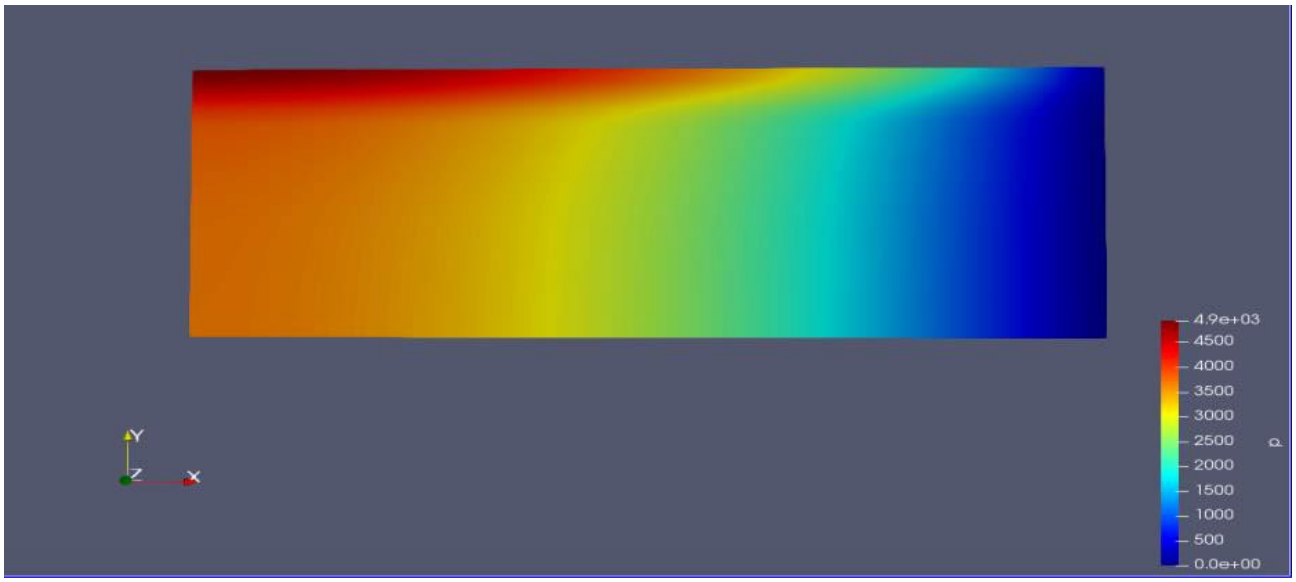

Figure 21. *Pressure profile of Initial case in ParaView software.*

In Figure 22 are represented the pressure profiles in each zone and in the top surface of the AC along x axis.

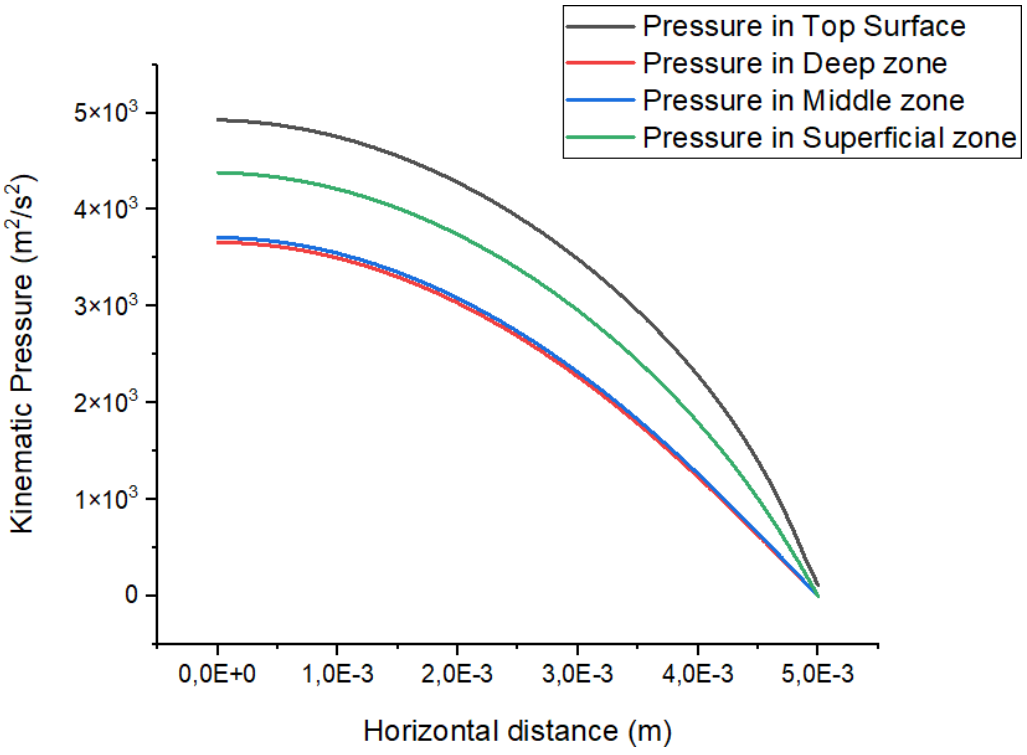

Figure 22. *Pressure profile of Initial case for each AC zone.*

4.2.3 Results of Velocity Profile

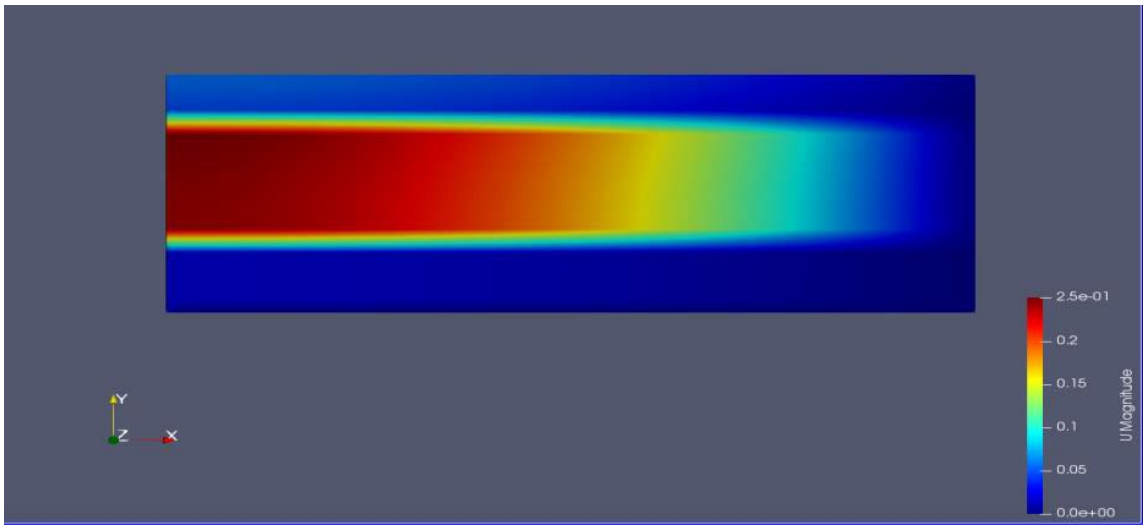

Figure 23. *Magnitude of Velocity Profile in ParaView software*

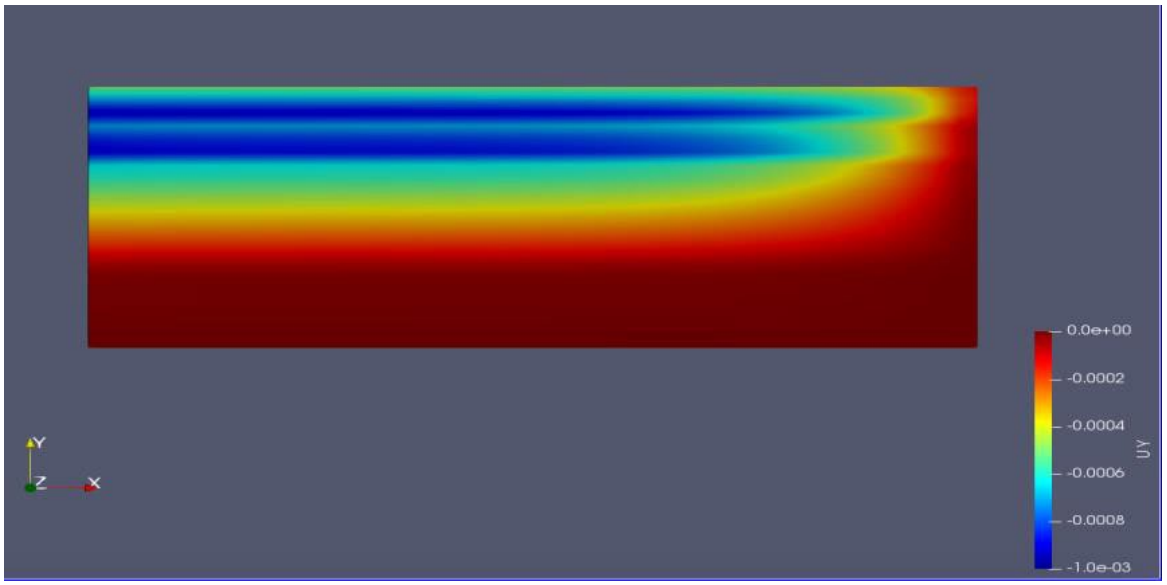

Figure 24. *Velocity Profile in y axis in ParaView software.*

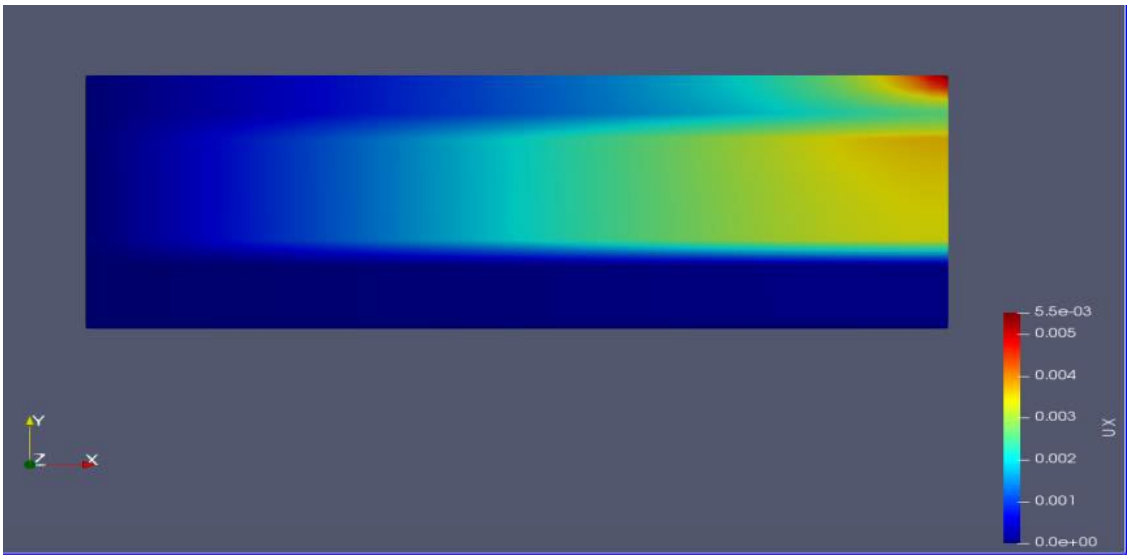

Figure 25. *Velocity Profile in x axis in ParaView software.*

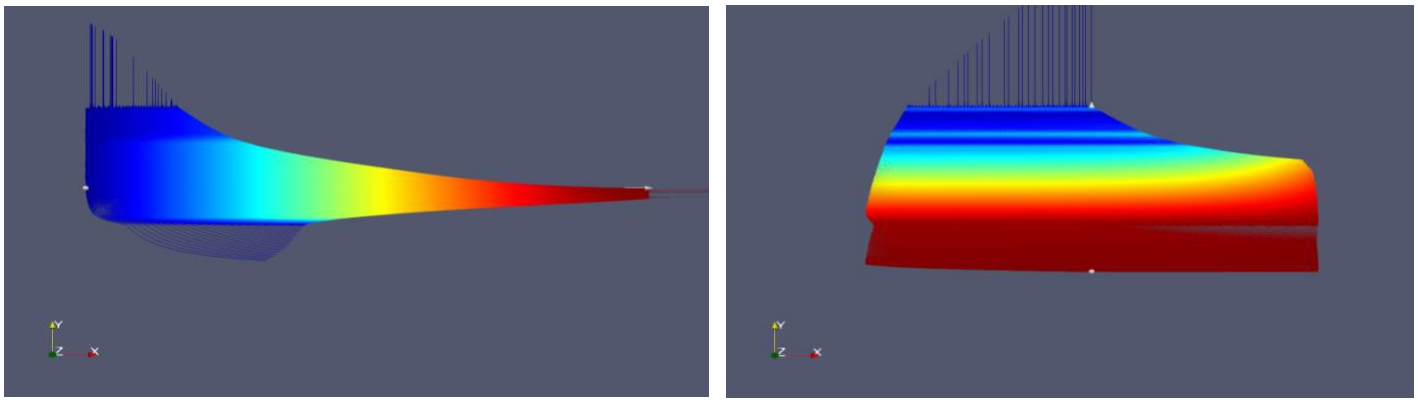

Figure 26. *Velocity Glyph in x direction (left) and y direction (right).*

4.3 Comparison between Isotropic & Anisotropic Porous Medium

After calculating the pressure profile for an isotropic porous medium (AC) and an anisotropic case with three different zones that actually AC has, the results were compared in the following graph in order to study the effect of anisotropy permeability in AC. As is shown, due to the different orientation of fibers in each zone and the anisotropy of permeability, pressure values are much lower in Initial case.

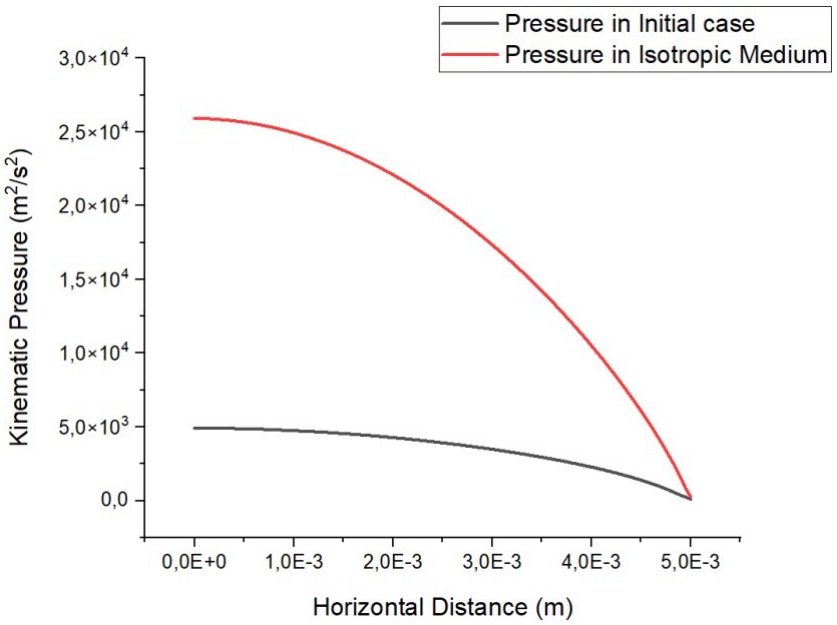

Figure 27. *Comparison Graph between isotropic and anisotropic case.*

Below in Figure 27 & 28 the profile of pressure and velocity is shown for the isotropic case (one zone) of AC.

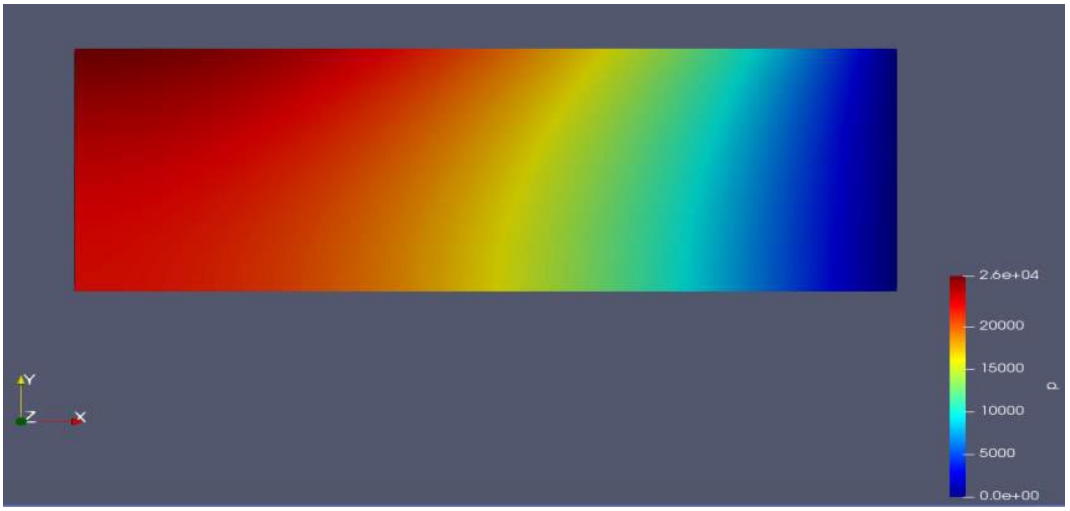

Figure 28. *Pressure profile of isotropic case in ParaView software.*

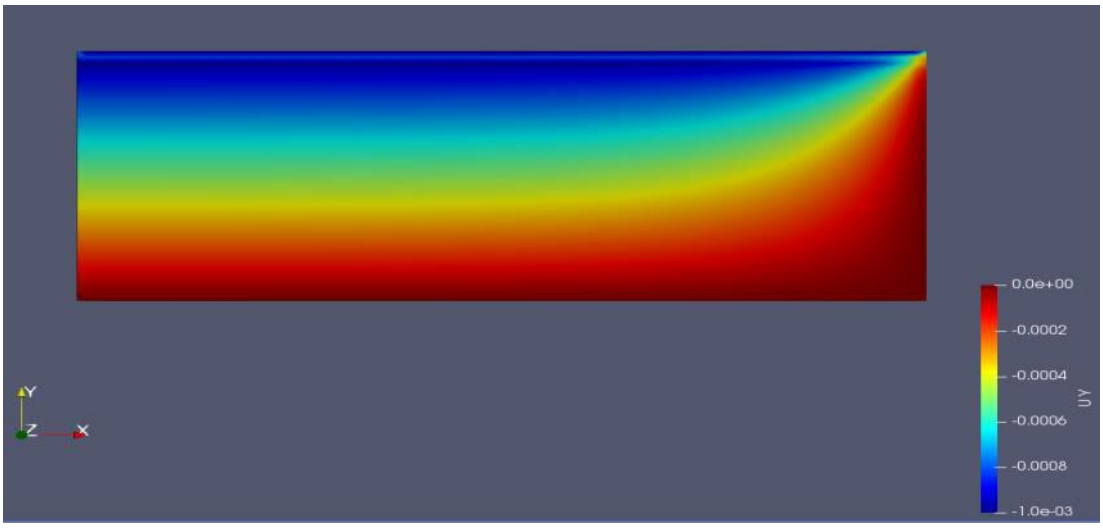

Figure 29. *Velocity in y axis profile of Isotropic case in ParaView software.*

4.4 Force distribution according to thickness of zones

In the final part of this study the effect of the thickness of each zone was investigated. To achieve that, several simulations were performed in OpenFOAM according to literature review and Table 3 for the broad of thickness in each zone of AC. After the pressure profile on the top of the surface of superficial zone was visualized, we used the data, and the total force was calculated form the integration of pressure along x-axis. Below in Table 11 is shown the Total Force according to each superficial zone thickness and we can see the comparison of the results in Figure 30.

Table 8. *Simulations for different zone thickness.*

T_sup (%)	T_middle (%)	T_deep (%)	Force (N)
20	50	30	**17,52115637**
19	54	27	**17,27458917**
17	60	23	**16,22571734**
10	59	31	**15,12514681**
13	58	29	**16,03946166**
16	55	29	**16,83768558**
14	56	30	**16,4671039**
20	50	30	**18,0006159**

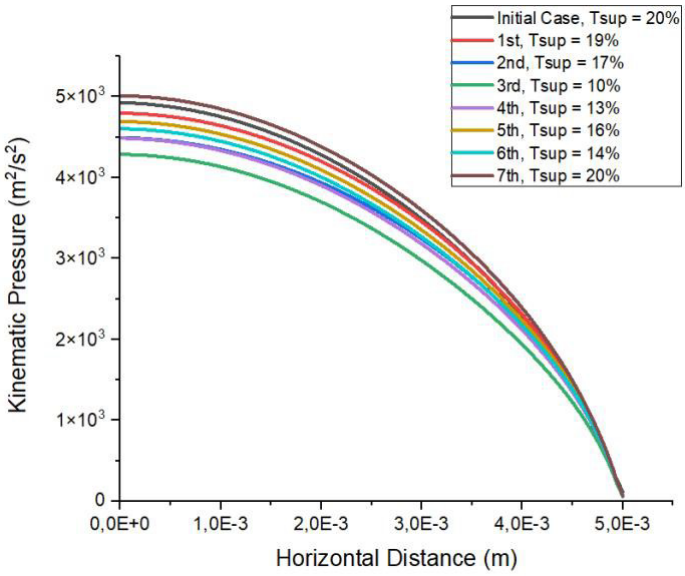

Figure 30. *Pressure profile in different thickness percentage of each zone.*

CHAPTER 5. CONCLUSIONS – SUGGESTIONS FOR FURTHER STUDY

As described in the present Chapter, analytical solution of a porous medium and porous models were developed, in order to examine the effect of permeability in the pressure profile of an Articular Cartilage (AC) and to test the validity of the porousSimpleFoam solver through comparison with the analytical data that were obtained. Anisotropy of the permeability in a porous medium is a consequence of the orientation of the fibers and plays a significant role in AC behavior. The first part of the process involved the development of the analytical solution of the flow through an isotropic porous medium with the appropriate equations and conditions of the problem. The second part of the procedure included the creation of an anisotropic model with three porous zones that represents AC and the simulation of several cases in order to examine the differences in the generation of pressure and therefore in the force distribution on the top surface of AC. To achieve that a brief literature survey in the permeability models that have been demonstrated in the past years was conducted and the permeability models that have been used in the Thesis were analyzed in detail. The thickness of the cartilage zones plays also an important role in the pressure and consequently in the force distribution in the top surface of the AC and several cases of different zone thickness have been simulated and compared.

Based on the above conclusions, and considering the limitations of the study, future investigations can be proposed, aiming to a more profound and complete understanding of the effect of anisotropy permeability in AC. Osteoarthritis (OA) is a degenerative disease that affects the entire knee joint. One factor is defined by a progressive degenerative erosion of the AC, in addition to subchondral bone alterations, joint pain, and discomfort. The Articular Cartilage that covers the ends of the bones in joints eventually deteriorates, resulting in OA. OA is associated with changes in the thickness of AC and increases in permeability. The thickness of the tissue grows in the early stages of OA and diminishes in the later stages. Understanding the contact mechanics of diseased AC could lead to new insights into the adaptive and degenerative mechanisms that lead to joint degeneration and osteoarthritis.

REFERENCES

[1] H. Y. Ng, A. A. Lee, and K. X. Shen, " “Articular Cartilage: Structure, Composition, Injuries and Repair,”," *JSM Bone and Joint Dis,* Vols. vol. 1, no. 2, p. p. 1010, 2017.

[2] Joerg Eschweiler, Nils Horn, Bjoern Rath, Marcel Betsch, Alice Baroncini, Markus Tingart, and Filippo Migliorini, "The Biomechanics of Cartilage—An Overview," 2021 Apr 1.

[3] A. M. Bhosale and J. B. Richardson, , "“Articular cartilage: Structure, injuries and review of management,”," *British Medical Bulletin,* Vols. vol. 87, no. 1, p. pp. 77–95, Sep. 2008,.

[4] A. J. S. Fox, A. Bedi, and S. A. Rodeo,, " “The Basic Science of Articular Cartilage: Structure, Composition, and Function,”," 2009, doi: 10.1177/1941738109350438..

[5] L. Zhang, J. Hu, and K. A. Athanasiou,, " “The Role of Tissue Engineering in Articular Cartilage Repair and Regeneration.”," *Crit Rev Biomed Eng,* 2009.

[6] Fetter, C. W. (Charles Willard), Contaminant hydrogeology / C.W. Fetter., 1999.

[7] J. Eschweiler et al.,, "“life The Biomechanics of Cartilage-An Overview,”," 2021, doi: 10.3390/life11040302..

[8] L. Tufts et al.,, " “Correlating high-resolution magic angle spinning NMR spectroscopy and gene analysis in osteoarthritic cartilage,”," *NMR in Biomedicine,* Vols. vol. 28, no. 5, p. pp. 523–528, May 2015.

[9] T. Farquhar, P. R. Dawson, and P. A. Torzilli,, " “A Microstructural Model for the Anisotropic Drained Stiffness of Articular Cartilage,”," *Journal of Biomechanical Engineering,* Vols. vol. 112, no. 4, p. pp. 414–425, Nov. 1990.

[10] M. Fortin, J. Soulhat, A. Shirazi-Adl, E. B. Hunziker, and M. D. Buschmann, " “Unconfined Compression of Articular Cartilage: Nonlinear Behavior and Comparison With a Fibril-Reinforced Biphasic Model,”," *Journal of Biomechanical Engineering,* Vols. vol. 122, no 2, pp. pp. 189-195, Apr. 2000.

[11] T. C. Gasser, R. W. Ogden, and G. A. Holzapfel, " “Hyperelastic modelling of arterial layers with distributed collagen fibre orientations”,".

[12] Salvatore Federico and Walter Herzog, On the anisotropy and inhomogeneity of permeabilityin articular cartilage, 2007.

[13] Mow VC, Kuei SC, Lai WM, Armstrong , CG: Biphasic creep and stress relaxation of articular cartilage in compression. Theory and experiments. / Biomech Eng 102:73-84, 1980.

[14] A. R. Gannon, T. Nagel, and D. J. Kelly,, " “The role of the superficial region in determining the dynamic properties of articular cartilage,”," *Osteoarthritis and Cartilage,* Vols. vol. 20, no. 11, p. pp. 1417–1425, Nov. 2012.

[15] Maroudas A, Wachtel E, Grushko G, et al, The effects of osmotic and mechanical pressure on water and partitioning in articular cartilage. Biochem Biophys Acta, 1991.

[16] J. Clark, The organisation of collagen fibrils in the superficial zones of articular cartilage, 1990.

[17] M.J. Kaab, I.A. Gwynn and H.P. Notzli, Collagen fibre arrangement in the tibial plateau articular cartilage of man and other mammalian species, 1998.

[18] H. Ng, K. A. Lee, Yu-Fang Shen, "Articular Cartilage : Structure , Composition , Injuries and Repair," 2017.

[19] DS Clague, BD Kandhai, R Zhang, Peter MA Sloot, "Hydraulic permeability of (un) bounded fibrous media using the lattice Boltzmann method," 2000/1/1.

[20] R.M. Schinagl, D. Gurskis, A.C. Chen and R.L. Sah, Depth-dependent confined compression modulus of full-thickness bovine articular cartilage, 1997.

[21] B. R. Gebart, Permeability of Unidirectional Reinforcements for RTM, 1990.

[22] Salvatore Federico , Alfio Grillo, Guido La Rosa, Gaetano Giaquinta, Walter Herzog, "A transversely isotropic, transversely homogeneous microstructural-statistical model of articular cartilage," *J Biomech,* 2005 Oct.

[23] M. A. Biot, "Mechanics of deformation and acoustic propagation in porous media," *Journal of Applied Physics,* pp. pp.1482-1498, 1962.

[24] M H Holmes, V C Mow, "The nonlinear characteristics of soft gels and hydrated connective tissues in ultrafiltration," *J Biomech.,* 1990.

[25] Gerard A. Ateshian and Huiqun Wang, A THEORETICAL SOLUTION FOR THE FRICTIONLESS ROLLING CONTACT OF CYLYNDRICAL BIPHASIC ARTICULAR CARTILAGE LAYERS, 1995.

[26] H. H, On the periodic fundamental solutions of the Stokes equations and their application to viscous flow past a cubic array of spheres, J. Fluid Mech. 5, 1959.

[27] Murakami, T., et al., Adaptive multimode lubrication in natural synovial joints and artificial joints, 2017.

[28] S. OLSEN, and A. OLOYEDE, A Finite Element Analysis Methodology for Representing theArticular Cartilage Functional Structure, 2002.

[29] J.Z. Wu, W. Herzog*, M. Epstein, Evaluation of the finite element software ABAQUS for biomechanical modelling of biphasic tissues, 1997.

[30] L. P. Li, M. D. Buschmann, and A. Shirazi-Adl, "“A fibril reinforced nonhomogeneous poroelastic model for articular cartilage: inhomogeneous response in unconfined compression"," *Journal of Biomechanics ,* Vols. vol. 33, no. 12, p. pp. 1533–1541, Dec. 2000, doi: 10.1016/S0021-9290(00)00153-6..

[31] R. L. SPILKER, AND J - K. SUH, Formulation And Evaluation of a Finite Element Model for the Biphasic Model of Hydrated Soft Tissues, 1990.

[32] Erisken C, Tsiantis A, Papathanasiou TD, Karvelas EG., "Collagen fibril diameter distribution affects permeability of ligament tissue: A computational study on healthy and injured tissues.," *Comput Methods Programs Biomed. ,* p. doi: 10.1016/j.cmpb.2020.105554., 2020 Nov;196:105554..

[33] Zeman Liu,Yiqi Wang, ORCID and Fei Guo , "An Investigation into Hydraulic Permeability of Fibrous Membranes with Nonwoven Random and Quasi-Parallel Structures," *Electrospun Nanofiber Membranes: From Synthesis to Applications,* 2022, 12(1), 54; https://doi.org/10.3390/membranes12010054.

[34] Mohamad Karaki, Ayman Hallal, Rafic younes, Francois Trochu, Pascal Lafon, et al., "A Comparative Analytical, Numerical and Experimental Analysis of the Microscopic Permeability of Fiber Bundles in Composite Materials," *International Journal of Composite Materials, Scientific & Academic Publishing,* pp. pp.82-102, 2017.

[35]]. R. Sullivan, Specific surface measurements on compact bundles of parallel fibers, J. Appl. Phys. 13, 1942.

[36] S. Kuwabara, The forces experienced by randomly distributed parallel circular cylinders or spheres in a viscous flow at small Reynolds numbers, J. Phys. Soc. Jpn. 14, 1959.

[37] J. Happel and H. Brenner, Low Reynolds number hydrodynamics: with special applications to particulate media, 31 August 1973.

[38] E. M. Sparrow,A. L. Loeffler JR., "Longitudinal laminar flow between cylinders arranged in regular array," *Aiche Journal,* September 1959.

[39] J. Happel, Viscous flow relative to arrays of cylinders, AIChE 5, 1959.

[40] A.S. Sangani, A. Acrivos, Slow flow past periodic arrays of cylinders with application to heat transfer, Int. J. Multiphase Flow 8, 1982.

[41] J. E. Drummond and M. I. Tahir, "Laminar viscous flow through regular arrays of parallel solid cylinders", Int. J. Multiphase Flow 10, 515, 1983.

[42] M. v. Bruschke and S. G. Advani, , "“Flow of generalized Newtonian fluids across a periodic array of cylinders”," *Journal of Rheology,* Vols. vol. 37, no. 3, p. p. 479, Jun. 1998, doi: 10.1122/1.550455.

[43] A. Tamayol, M. Bahrami, Analytical determination of viscous permeability of fibrous porous media, 2008.

[44] MANOLIS M. TOMADAKIS, TERI J. ROBERTSON, Viscous permeability of random fiber Structures: Comparison of Electrical and Diffusional Estimates with Experimental and Analytical Results, 2003.

[45] M. A. Tahir and H. Vahedi Tafreshi, Influence of fiber orientation on the transverse permeability of fibrous media, 2009.

[46] Triantafyllos Stylianopoulos,1 Andrew Yeckel,1 Jeffrey J. Derby, Xiao-Juan Luo, Mark S. Shephard, Edward A. Sander, and Victor H. Barocas, Permeability calculations in three-dimensional isotropic and oriented fiber networks, 2008.

[47] David S. Clague and Ronald J. Phillips, A numerical calculation of the hydraulic permeability of three-dimensional, 1996.

[48] T.D.Papathanasiou, "A structure-oriented micromechanical model for viscous flow through square arrays of

fibre clusters," *Composites Science and Technology,* vol. Volume 56, no. Issue 9, pp. Pages 1055-1069, 1996.

[49] T.D.Papathanasiou, "On the effective permeability of square arrays of permeable fiber tows," *International Journal of Multiphase Flow,* vol. Volume 23, no. Issue 1, pp. Pages 81-92, February 1997.

[50] T.D. Papathanasiou, "A Structure-Oriented Micromechanical Model for Viscous Flow Through Square Arrays of Fibre Clusters," *Composites Science and Technology,* pp. 1055-1069, December 1996.

[51] T.D. Papathanasiou, "Flow across structured fiber bundles: a dimensionless correlation," *International Journal of Multiphase Flow,* vol. Volume 27, no. Issue 8, pp. Pages 1451-1461, August 2001.

[52] T. D. Papathanasiou, E. M. Gravel, S. C. Barwick, E. D. Dendy, "Non-Isotropic structured fibrous media: The permeability of arrays of fiber bundles of elliptical cross section," *Polymer Composites,* vol. Volume 23, no. Issue 4, pp. Pages 520-529, 15 April 2004.

[53] Xiaoming Chen & Thanasis D. Papathanasiou, "The transverse permeability of disordered fiber arrays: a statistical correlation in terms of the mean nearest interfiber spacing," *Transport in Porous Media,* 71 (2), 233-251, 2008.

[54] Xiaoming Chen, T.D. Papathanasiou, "Micro-scale modeling of axial flow through unidirectional disordered fiber arrays," *Composites Science and Technology,* 67 (7-8), 1286-1293, 2007.

[55] X Chen, TD Papathanasiou, "On the variability of the Kozeny constant for saturated flow across unidirectional disordered fiber arrays," *Composites Part A: Applied Science and Manufacturing,* 7 (6), 836-846, 2006.

[56] SC Barwick, TD Papathanasiou, " Identification of fiber misalignment in continuous fiber composites," *Polymer composites 24 (3), 475-486, 2003.*

[57] TD Papathanasiou, B Markicevic, ED Dendy, " A computational evaluation of the Ergun and Forchheimer equations for fibrous porous media,," *Physics of Fluids 13 (10), 2795-2804, 2001.*

[58] B Markicevic, TD Papathanasiou, "On the apparent permeability of regular arrays of nonuniform fibers,," *Physics of Fluids 14 (9), 3347-3349, 2002.*

[59] TD Papathanasiou, "The hydraulic permeability of periodic arrays of cylinders of varying size," *Journal of Porous Media 4 (4), 2001.*

[60] A. Maroudas and P. Bullough, ""“Permeability of Articular Cartilage”," *Nature 1968 219:5160,* Vols. vol. 219, no. 5160, p. pp. 1260–1261.

[61] S. Han et al., , ""“Changes in ADC Caused by Tensile Loading of Rabbit Achilles Tendon: Evidence for Water Transport,”," *Journal of Magnetic Resonance,* Vols. vol. 144, no. 2, p. pp. 217–227, Jun. 2000, doi: 10.1006/JMRE.2000.2075.

[62] J. Wellen, K. G. Helmer, P. Grigg, and C. H. Sotak, " “Application of porous-media theory to the investigation of water ADC changes in rabbit Achilles tendon caused by tensile loading,”," *Journal of Magnetic Resonance,* Vols. vol. 170, no. 1, p. pp. 49–55, Sep. 2004.